MATHEMATICAL MODELS OF CHEMICAL REACTIONS: DISCREPANCIES BETWEEN MARKOV CHAINS AND MASS ACTION KINETICS

by

Parker L. Childs

A dissertation submitted to the faculty of
The University of Utah
in partial fulfillment of the requirements for the degree of

Doctor of Philosophy

Department of Mathematics

The University of Utah

May 2017

The University of Utah Graduate School

STATEMENT OF DISSERTATION APPROVAL

The dissertation of   **Parker L. Childs**

has been approved by the following supervisory committee members:

James P. Keener ,	Chair(s)	**22 July 2016**
		Date Approved
Frederick R. Adler ,	Member	**22 July 2016**
		Date Approved
David F. Blair ,	Member	**22 July 2016**
		Date Approved
Paul C. Bressloff ,	Member	**22 July 2016**
		Date Approved
Aaron L. Fogelson ,	Member	**22 July 2016**
		Date Approved

by **Peter E. Trapa** , Chair/Dean of

the Department/College/School of **Mathematics**

and by **David B. Kieda** , Dean of The Graduate School.

ABSTRACT

We analyze different models of several chemical reactions. We find that, for some reactions, the steady state behavior of the chemical master equation, which describes the continuous time, discrete state Markov process, is poorly approximated by the deterministic model derived from the law of mass action or a mean field model derived in a similar way.

We show that certain simple enzymatic reactions have bimodal stationary distributions in appropriate parameter ranges, though the deterministic and mean field models for these reactions do not have the capacity to admit multiple equilibrium points no matter the choice of rate constants. We provide power series expansions for these bimodal distributions.

We also consider several variants of an autocatalytic reaction. This reaction's deterministic model predicts a unique positive stable equilibrium, but the only stationary distribution of its chemical master equation predicts extinction of the autocatalytic chemical species with probability 1. We show that the transient distribution of this chemical master equation is centered near the deterministic equilibrium and that the stationary distribution is only reached on a much longer time scale.

Finally, we consider a model for the rotational direction switching of the bacterial rotary motor and propose two possible reductions for the state space of the corresponding Markov chain. One reduction, a mean field approximation, is unable to produce physically realistic phenomena. The other reduction retains the properties of interest in the system while significantly decreasing the computation required for analysis. We use this second reduction to fit parameters for the full stochastic system and suggest a mechanism for the sensitivity of the switch.

CONTENTS

LIST OF FIGURES

LIST OF TABLES

CHAPTER 1

INTRODUCTION

An important and long-standing question in the theory of chemical reaction networks has been whether, for a given chemical reaction network, there exists a set of rate constants corresponding to the reactions for which the corresponding set of nonlinear ordinary differential equations derived from the law of mass action has more than one equilibrium point. A host of advances on this topic was made over the course of many years [16, 10, 11, 12, 13, 14]. Major results from the work cited here include the Deficiency Zero Theorem and the Deficiency One Theorem. These theorems seek to classify reaction networks that admit multiple species concentration equilibria and those that do not. However, these theorems are inconclusive for many reaction networks.

Schlosser and Feinberg [27, 28] sought to fill in these gaps using a different tool, which they called the species-complex-linkage graph. But the species-complex-linkage graph still cannot provide the answer for many reaction networks. More recently, Craciun and Feinberg [3, 5, 6, 4] have developed even sharper tools for determining conditions under which the deterministic ordinary differential equations derived from the law of mass action can or cannot admit multiple equilibrium points. These more recent theorems, just like the older theorems, rely wholly on the topological structure of the reaction network. Craciun and Feinberg, however, defined two novel important objects associated with a chemical reaction network: the injectivity property and the species-reaction graph. They proved powerful theorems relating easily-checked properties of the species reaction graph to the injectivity of the network. These theorems eclipse the results from the species-complex-linkage graph approach in that any reaction that can be classified by the former can also be classified by the latter. But there are reaction networks for which the species-complex-linkage graph is inconclusive and the species-reaction graph provides a definitive result about injectivity.

None of the results from this branch of investigation, which may be called chemical reaction network theory, deal with possible inhomogeneities. By their very nature, the deterministic ODEs derived from the law of mass action can only exist under the assumptions that (1) concentrations of reactants and products in the system are continuous variables that can assume any nonnegative finite value and (2) these concentrations are homogeneous throughout the volume of the system. Under certain

conditions, these assumptions may be good approximations of reality. If a reaction system occurs in a large enough volume, however, or if the number of particles participating in the reaction is small enough, these assumptions may not give an accurate, or even useful, picture of reality. One possible adjustment to this type of model is to allow the concentrations to be spatially inhomogeneous and add a diffusion term to the ODEs, turning them into PDEs. This type of model is useful in many circumstances, but it is still deterministic and still assumes that chemical concentrations as well as spatial gradients of them are continuous.

But, matter is discrete. Important chemical reactions in biology include transcription and translation of genes, or, as we discuss in Chapter 4, the rotation of individual molecular motors. Such motors, and genes, either DNA or RNA, often occur with extremely low copy numbers in individual cells [7, 24]. Thus, they are clearly not spatially homogeneous, nor does it make sense to think of them even as spatially varying concentrations at all. A different type of model is required, one which can account for stochastically fluctuating numbers of molecules.

There are several different ways to model chemical reactions in a nondeterministic fashion. Érdi and Tóth and, much more recently, Érdi and Lente have written expositions on the subject [9, 8]. The reader is encouraged to refer to these texts for a thorough introduction to the modeling of stochastic chemical reactions. The type of stochastic model that we use extensively in this work is the continuous time, discrete state model, which, if the process is Markovian, is called a continuous time Markov chain. This gives rise to the primary tool used throughout this text, the chemical master equation.

In this type of modeling, each state in the state space represents a particular configuration $(n_{A_1}, n_{A_2}, \ldots, n_{A_k})$ within which there are n_{A_i} molecules of each of the k species participating in the reaction A_i, $i = 1, \ldots, k$. For most reactions, this state space is very large. Often there are countably infinite states, and the connections between them may be highly reticulate. The chemical master equation is a system of first-order linear homogeneous ordinary differential equations that describes the continuous time evolution of probabilities assigned to each state in the state space. Hence, this system may have countably many equations, a fact that implies it may

not be possible to find exact time-dependent solutions.

In the 1970s Kurtz [18, 19, 20] provided the classical result that the continuous time, discrete state model converges to the deterministic model in the infinite volume limit. A classification of reactions that can be accurately modeled by deterministic models when occurring in a finite volume would be very useful. We are not the first to construct examples of reactions whose deterministic model predictions are qualitatively different than the continuous state stochastic process obtained by introducing noise (usually called the Langevin equation) [26, 15, 22] or the chemical master equation [17, 29, 23, 1, 25]. As yet, there is no unifying theory to catalog these reactions. In this dissertation, we illustrate a few certain reactions whose chemical master equation predicts different behavior than the deterministic model. We also consider mean-field models for some of these processes, and show that in certain cases, this model is equivalent to the deterministic mass action model.

In Chapter 2 we consider a classic enzymatic reaction [21] coupled with different types of inhibition of the enzyme acting in the reaction. We find that the stationary distributions of the chemical master equations for these reactions are attained on a time scale that is easily simulated. However, under certain conditions, these stationary distributions have the capacity to be multimodal, though the corresponding deterministic models do not have the capacity for multiple equilibrium points no matter the rate constants assigned to the reactions.

In Chapter 3 we explore several variants of an autocatalytic reaction proposed by Keizer [17] as a cautionary tale against accepting the stationary distribution of the chemical master equation without further investigation of the time-dependent solution. We find that expected times for the processes to reach their absorbing states are exponentially large in certain parameters intrinsic to the reaction system.

Finally, in Chapter 4, we discuss a mathematical model of the rotary motor found in many different bacterial species. This motor is able to switch its direction of rotation with remarkable speed and sensitivity to a certain intracellular chemical signal [2]. Though this is a different type of chemical reaction than the others studied here, it is a reaction nonetheless, and has an associated chemical master equation. The law of mass action is not applicable to this reaction since not all of the species

involved are freely diffusing, however we discuss a mean field approach to this model and illustrate why it does not produce a reliable prediction of the behavior of the motor.

A crucial tool used in Chapters 3 and 4 is the reduction of the size of the state space. The methods for doing this are ad hoc. There is no general method for reducing the size or dimension of a stochastic state space without first considering the structure of the space itself. We find peculiar features of these systems which we exploit to appropriately cluster or eliminate states while retaining the important properties we wish to analyze. In Chapter 2, we effectively split the state space into appropriate pieces that communicate with one another. It is not a reduction, but, in a similar way, it simplifies the necessary calculations.

1.1 References

[1] L. M. Bishop and H. Qian, *Stochastic bistability and bifurcation in a mesoscopic signaling system with autocatalytic kinase*, Biophys. J., 98 (2010), pp. 1–11.

[2] P. Cluzel, M. Surette, and S. Leibler, *An ultrasensitive bacterial motor revealed by monitoring signaling proteins in single cells*, Science, 287 (2000), pp. 1652–1655.

[3] G. Craciun and M. Feinberg, *Multiple equilibria in the complex chemical reaction networks: I. The injectivity property*, SIAM J. Appl. Math., 65 (2005), pp. 1526–1546.

[4] ——, *Multiple equilibria in the complex chemical reaction networks: Extensions to entrapped species models*, IEE Proc. Systems Biol., 153 (2006), pp. 179–186.

[5] ——, *Multiple equilibria in the complex chemical reaction networks: II. The species-reaction graph*, SIAM J. Appl. Math., 66 (2006), pp. 1321–1338.

[6] G. Craciun, Y. Tang, and M. Feinberg, *Understanding bistability in complex enzyme-driven reaction networks*, PNAS, 103 (2006), pp. 8697–8702.

[7] M. B. Elowitz, A. J. Levine, E. D. Siggia, and P. S. Swain, *Stochastic gene expression in a single cell*, Science, 297 (2002), pp. 1183–1186.

[8] P. Érdi and G. Lente, *Stochastic Chemical Kinetics: Theory and (Mostly) Systems Biological Applications*, Springer Series in Synergetics, Springer, New York, 2014.

[9] P. Érdi and J. Tóth, *Mathematical Models of Chemical Reactions: Theory and Applications of Deterministic and Stochastic Models*, Princeton University Press, New Jersey, 1989.

[10] M. Feinberg, *Lectures on Chemical Reaction Networks*. Delivered at the Mathematics Research Center, University of Wisconsin-Madison. Available for download at https://crnt.osu.edu/LecturesOnReactionNetworks, 1979.

[11] ——, *Chemical reaction network structure and the stability of complex isothermal reactors–I. The deficiency zero and deficiency one theorems*, Chem. Eng. Sci., 42 (1987), pp. 2229–2268.

[12] ——, *Chemical reaction network structure and the stability of complex isothermal reactors–II. Multiple steady states for networks of deficiency one*, Chem. Eng. Sci., 43 (1988), pp. 1–25.

[13] ——, *Necessary and sufficient conditions for detailed balancing in mass action systems of arbitrary complexity*, Chem. Eng. Sci., 44 (1989), pp. 1819–1827.

[14] ——, *The existence and uniqueness of steady states for a class of chemical reaction networks*, Arch. Rational Mech. Anal., 132 (1995), pp. 311–370.

[15] J. Goutsias, *Classical versus stochastic kinetics modeling of biochemical reaction systems*, Biophys. J., 92 (2007), pp. 2350–2365.

[16] F. Horn, *Necessary and sufficient conditions for complex balancing in chemical kinetics*, Arch. Rational Mech. Anal., 49 (1972), pp. 172–186.

[17] J. Keizer, *Statistical Thermodynamics of Nonequilibrium Processes*, Springer-Verlag, New York, 1987.

[18] T. G. Kurtz, *Solutions of ordinary differential equations as limits of pure jump Markov processes*, J. Appl Probab., 7 (1970), pp. 49–58.

[19] ——, *Limit theorems for sequences of jump markov processes approximating ordinary differential processes*, J. Appl Probab., 8 (1971), pp. 344–356.

[20] ——, *The relationship between stochastic and deterministic models for chemical reactions*, J. Chem. Phys., 57 (1972), pp. 2976–2978.

[21] L. Michaelis and M. L. Menten, *Die kinetik der invertinwirkung*, Biochemische Zeitschrift, 49 (1913), pp. 333–369.

[22] C. A. Miller and D. A. Beard, *The effects of reversibility and noise on stochastic phosphorylation cycles and cascades*, Biophys. J., 95 (2008), pp. 2183–2192.

[23] I. Nåsell, *Extinction and quasi-stationarity in the Verhulst logistic model*, J. Theor. Biol., 211 (2001), pp. 11–27.

[24] J. Paulsson, *Models of stochastic gene expression*, Phys. Life Rev., 2 (2005), pp. 157–175.

[25] H. Qian and L. M. Bishop, *The chemical master equation approach to nonequilibrium steady-state of open biochemical systems: Linear single-molecule enzyme kinetics and nonlinear biochemical reaction networks*, Int. J. Mol. Sci., 11 (2010), pp. 3472–3500.

[26] M. Samoilov, S. Plyasunov, and A. P. Arkin, *Stochastic amplification and signaling in enzymatic futile cycles through noise-induced bistability with oscillations*, PNAS, 102 (2005), pp. 2310–2315.

[27] P. M. Schlosser, *A Graphical Determination of the Possibility of Multiple Steady States in Complex Isothermal CFSTRs*, PhD thesis, University of Rochester, Rochester, NY, 1988.

[28] P. M. Schlosser and M. Feinberg, *A theory of multiple steady states in isothermal homogeneous CFSTRs with many reactions*, Chem. Eng. Sci., 49 (1994), pp. 1749–1767.

[29] M. Vellela and H. Qian, *A quasistationary analysis of a stochastic chemical reaction: Keizer's paradox*, Bull. Math. Biol., 69 (2007), pp. 1727–1746.

CHAPTER 2

INHIBITED ENZYME REACTIONS

An enzyme is a molecule that catalyzes, or lowers the energy required, for a chemical reaction to take place without itself being changed or consumed in the reaction. The reactants in such a reaction are called substrates, and, in the reaction, they are converted to products. Countless examples of enzymatic reactions occur in nature. They are crucial for the existence of life. Therefore, understanding their properties and general behavior is important for understanding many biological processes.

For over 100 years, people have been striving to understand the kinetics of enzymatic chemical reactions. It was 1913 when Michaelis and Menten published their classic result about the invertase-catalyzed conversion of sucrose to its cleavage products fructose and glucose [6]. Tens of thousands of experiments have been performed and papers published on the topic of enzyme kinetics. Another classic mathematical result on the subject is that found by Goldbeter and Koshland [5]. They showed, using a deterministic model, the existence of an ultrasensitive switch between the unmodified and modified form of a protein when its interconversion is catalyzed by two different enzymes. Much more recently, it has been shown that including external noise in the Goldbeter-Koshland reactions can induce bistability in the expected output of the system [8, 7]. All the results just mentioned and the vast majority of similar studies treat the concentrations of chemical species in the volume within which the reactions take place as continuous variables.

In this chapter we consider three different simplified variations of an enzymatic reaction in which the enzyme can be inhibited from acting in the reaction. The first of these is a very simple competitive inhibition. The second and third reactions are cases where the product of the reaction acts as the inhibitor, and, hence, downregulates its own production. The difference between the second and third reactions is that the second has a reverse reaction which gives rise to a conservation law. In the third reaction, we eliminate the reverse reaction to allow for slightly more general conditions.

2.1   Initial Reaction Network

We begin by considering the following chemical reaction network.

$$E + S \rightleftarrows ES \rightarrow E + P$$
$$E + I \rightleftarrows EI \tag{2.1}$$

This reaction is our "example zero," in that we do not analyze it in the same depth as we do the others. This particular reaction is relevant to our discussion because this reaction network, along with several other similar networks, has been shown to not have the possibility of multiple equilibria for any set of positive rate constants when modeled using mass-action kinetics[1, 2, 3]. However, numerical experiments using Gillespie simulations indicate that for certain parameter regimes and certain initial concentrations there are multiple basins of attraction. Figure 2.1 shows a scatterplot of the fraction of time the system had a given number of product molecules over the course of a simulation, and Table 2.1 lists the parameters required to generate this simulation. This plot clearly shows a bimodal distribution. In order to gain a better understanding of this type of steady state behavior, we consider a similar, but simpler network.

2.2   Initial Modified Reaction Network

We begin by assuming that our reactions occur in a closed environment; there is no feed stream and no outflow. The reactions we consider here are the following:

$$E + S \rightarrow E + P$$
$$E + I \rightleftarrows EI \tag{2.2}$$
$$P \rightarrow S$$

This system arises by making two modifications of (2.1). The first modification is to remove the intermediate step of forming a complex. Instead, we allow S to be converted to P by E in one step. This modification may not be a realistic assumption for any particular biological or chemical process. However, it allows for analytical results which would, otherwise, be relatively intractable. The second modification, the addition of the last reaction in (2.2), mimics removal, or outflow, of the species P and inflow of the species S, but does so in a way that the total number of molecules
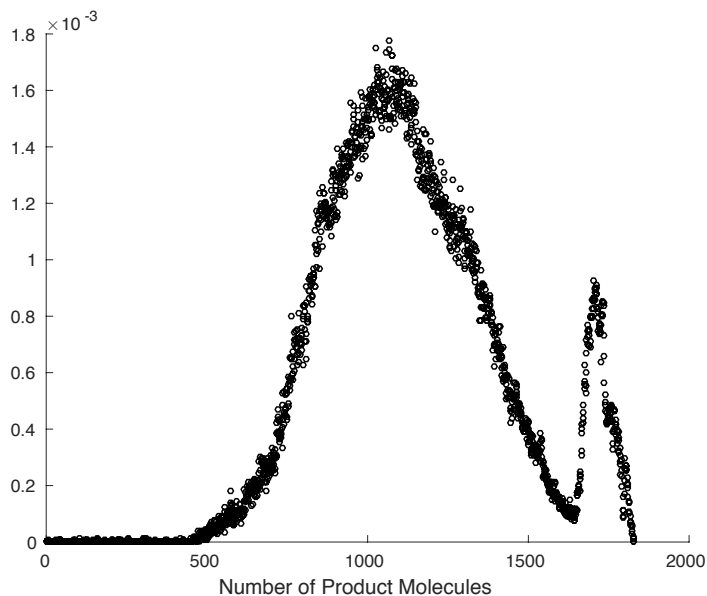
Figure 2.1. Simulation results for original inhibited enzyme reaction. Results of a Gillespie simulation of reaction network (2.1). The plots show the distribution of the fraction of time spent in each state over 300 time units. The parameters are taken from the section of the appendix of [3] for Table 1, Entry 4 with some exceptions. First, we do not include every reaction from this entry. The reactions not listed here have effective rate constant 0. Secondly, bimolecular rates and supply rates must be scaled by Volume^{-1} or Volume respectively. (here Volume $= 1$). Third, in order to get this bimodal distribution, we have scaled the original rates thus: $k_{E+S \to ES}$ by a factor of $1/20$, $k_{E+I \to EI}$ by a factor of 1000, and $k_{EI \to E+I}$ by a factor of $1/1000$. All the parameters used for this figure are listed in Table 2.1

of P and S are conserved. These modifications constrain the system, but Gillespie simulations indicate two attractor basins similar to those for (2.1).

It is especially interesting, again, to observe bimodality in the simulations, because, if we make the further assumption that I is in abundance compared to the total amount of enzyme, either freely active or inhibited, then it can be easily shown that under the law of mass-action the deterministic model only has one nonnegative steady state regardless of the reaction rate constants. We show this claim as follows.

2.2.1 Deterministic Model

If we let c_X be the concentration of species X, then the deterministic equations for 2.2 are as follows:

Table 2.1. Parameters used for Figure 2.1.

$k_{E+S \to ES}$	$25979.537/20$
$k_{ES \to E+S}$	3.3722455
$k_{ES \to E+P}$	5844.999
$k_{E+I \to EI}$	5.3341555×1000
$k_{EI \to E+I}$	$16623.325/1000$
$k_{\emptyset \to S}$	1734.2661
$k_{\emptyset \to I}$	1
$k_{S \to \emptyset}$	1
$k_{I \to \emptyset}$	1
$k_{P \to \emptyset}$	1

$$
\begin{aligned}
\dot{c}_S &= -k_{E+S \to E+P}\, c_E\, c_S + k_{P \to S}\, c_P, \\
\dot{c}_P &= k_{E+S \to E+P}\, c_E\, c_S - k_{P \to S}\, c_P, \\
\dot{c}_E &= -k_{E+I \to EI}\, c_E + k_{EI \to E+I}\, c_{EI}, \\
\dot{c}_{EI} &= k_{E+I \to EI}\, c_E - k_{EI \to E+I}\, c_{EI}.
\end{aligned}
\tag{2.3}
$$

We do not track the change in the concentration c_I because of the assumption that it is much greater than $c_E + c_{EI}$. Instead, it is absorbed into the rate constant $k_{E+I \to EI}$. Now, notice that $\dot{c}_S + \dot{c}_P = \dot{c}_E + \dot{c}_{EI} = 0$. This gives the two conservation equations $c_S + c_P = c_{S_T}$ and $c_E + c_{EI} = c_{E_T}$. Hence, (2.3) reduces to the two-variable system

$$
\begin{aligned}
\dot{c}_P &= -\left(k_{E+S \to E+P}\, c_E + k_{P \to S} \right) c_P + k_{E+S \to E+P}\, c_{S_T}\, c_E, \\
\dot{c}_E &= -\left(k_{E+I \to EI} + k_{EI \to E+I} \right) c_E + k_{EI \to E+I}\, c_{E_T},
\end{aligned}
\tag{2.4}
$$

which has the unique steady state

$$
\begin{aligned}
c_E^* &= \frac{k_{EI \to E+I}\, c_{E_T}}{k_{E+I \to EI} + k_{EI \to E+I}}, \\
c_P^* &= \frac{k_{E+S \to E+P}\, c_E^*\, c_{S_T}}{k_{E+S \to E+P}\, c_E^* + k_{P \to S}}.
\end{aligned}
\tag{2.5}
$$

We contrast this result with the steady state distributions obtained from the chemical master equation. To do so, we consider the simplest possible case, i.e. when there is only one enzyme molecule in the volume within which the reactions are occurring. It may be argued (and rightly so) that to treat the enzyme population as a concentration in this case is not reasonable, and, therefore, we should not expect

similar results as are given by the stochastic model with only one enzyme molecule. To answer this concern we first analyze what may be viewed as a more appropriate model.

2.2.2 Mean Field Model

The mean field model is similar to the deterministic mass-action model above. The substrate and product are still thought of as concentrations. Since there is only one enzyme molecule, though, we introduce the variable $p_A(t)$ which represents the probability that the enzyme is active (or uninhibited) at time t. The mean field equations are

$$\dot{c}_P = k_{E+S \to E+P}\, p_A\, (c_{S_T} - c_P) - k_{P \to S}\, c_P,$$
$$\dot{p}_A = -k_{E+I \to EI}\, p_A + k_{EI \to E+I}\, (1 - p_A). \tag{2.6}$$

We observe that the open interval $(0, 1)$ is invariant for p_A (as, indeed it must be) since $p_A = 0 \implies \dot{p}_A > 0$ and $p_A = 1 \implies \dot{p}_A < 0$. These equations are no different than (2.3), and, hence, this method of modeling the reaction can likewise only produce a unique steady state.

2.2.3 Stochastic Model

Now let us consider a fully stochastic and discrete description of reaction (2.2). As stated already, we consider the case with only one enzyme molecule in the volume within which the reactions are occurring. In this case it can either be in its free and active state or its inhibited state. We define n_X to be the number of molecules of species X and let $n_S + n_P = N$. Furthermore, we define

$$\mathbf{p}_j = \begin{pmatrix} p_{0,j} \\ p_{1,j} \\ \vdots \\ p_{N,j} \end{pmatrix}, \tag{2.7}$$

where $p_{i,j} = P(n_P = i, n_E = j)$. Then the chemical master equation is

$$\frac{d}{d\tau} \begin{pmatrix} \mathbf{p}_1 \\ \mathbf{p}_0 \end{pmatrix} = \begin{pmatrix} \alpha \mathbf{A} + \mathbf{B} - \beta \mathbf{I} & \gamma \mathbf{I} \\ \beta \mathbf{I} & \alpha \mathbf{A} - \gamma \mathbf{I} \end{pmatrix} \begin{pmatrix} \mathbf{p}_1 \\ \mathbf{p}_0 \end{pmatrix}, \tag{2.8}$$

where

$$\mathbf{A} = \begin{pmatrix} 0 & 1 & & & \\ & -1 & 2 & & \\ & & -2 & \ddots & \\ & & & \ddots & N \\ & & & & -N \end{pmatrix}, \quad \mathbf{B} = \begin{pmatrix} -N & & & & \\ N & -(N-1) & & & \\ & N-1 & \ddots & & \\ & & \ddots & -1 & \\ & & & 1 & 0 \end{pmatrix},$$

and $\mathbf{I}$ is the $(N+1) \times (N+1)$ identity. We have nondimensionalized this equation by scaling both sides by $\tilde{k}_{E+S \to E+P}^{-1}$. The tilde above this parameter indicates that it has been scaled by volume to correct units. This is of no consequence in comparing models, however, as volume can be set to any constant without changing any of the results herein. The nondimensional parameters in (2.8) are $\tau = \tilde{k}_{E+S \to E+P}\, t$, $\alpha = k_{P \to S}/\tilde{k}_{E+S \to E+P}$, $\beta = k_{E+I \to EI}/\tilde{k}_{E+S \to E+P}$, and $\gamma = k_{EI \to E+I}/\tilde{k}_{E+S \to E+P}$.

This system (2.8) is not difficult to solve analytically in steady state. We see that setting the left-hand side (LHS) to $\mathbf{0}$ yields

$$\mathbf{p}_1 = \beta^{-1} \left(\gamma \mathbf{I} - \alpha \mathbf{A} \right) \mathbf{p}_0 \tag{2.9}$$

with

$$\left(\beta^{-1}(\alpha \mathbf{A} + \mathbf{B} - \beta \mathbf{I})(\gamma \mathbf{I} - \alpha \mathbf{A}) + \gamma \mathbf{I} \right) \mathbf{p}_0 = \mathbf{0}. \tag{2.10}$$

However, this does not give us much intuition into how this distribution is affected by the parameters in the system. To gain this intuition we make several approximations.

2.2.3.1 Expansion in β

We first consider the case where β is a "small" parameter. What is meant by the word "small" here is made precise further on in this section. This assumption means the inhibition of enzyme occurs at a much slower rate than the conversion of substrate to product by enzyme. We can now approximate the steady state distribution as a power series in β. In steady state

$$\begin{pmatrix} \mathbf{p}_1 \\ \mathbf{p}_0 \end{pmatrix} = \begin{pmatrix} \mathbf{q}_0 \\ \mathbf{r}_0 \end{pmatrix} + \beta \begin{pmatrix} \mathbf{q}_1 \\ \mathbf{r}_1 \end{pmatrix} + O(\beta^2). \tag{2.11}$$

We impose the condition $\mathbf{1}^{\mathrm{T}}\mathbf{q}_k + \mathbf{1}^{\mathrm{T}}\mathbf{r}_k = \delta_{0,k}$ to ensure that the expansion is a probability distribution.

Then at $O(\beta^0)$ we have

$$(\alpha\mathbf{A} - \gamma\mathbf{I})\mathbf{r}_0 = \mathbf{0}. \tag{2.12}$$

For any $\alpha, \gamma > 0$, the matrix $\alpha\mathbf{A} - \gamma\mathbf{I}$ is upper triangular with strictly negative diagonal entries, hence it is invertible. Therefore $\mathbf{r}_0 = \mathbf{0}$. Also at $O(\beta^0)$ we have

$$(\alpha\mathbf{A} + \mathbf{B})\mathbf{q}_0 + \gamma\mathbf{r}_0 = (\alpha\mathbf{A} + \mathbf{B})\mathbf{q}_0 = \mathbf{0}. \tag{2.13}$$

It is straightforward to show that the elements of $\mathbf{q}_0$ are binomial with parameter $\frac{1}{1+\alpha}$. They are expressed simply as

$$\mathbf{q}_{0,i} = \binom{N}{i}\alpha^{N-i}(1+\alpha)^{-N}, \quad i = 0, \ldots, N. \tag{2.14}$$

At $O(\beta)$ we have

$$(\alpha\mathbf{A} - \gamma\mathbf{I})\mathbf{r}_1 + \mathbf{q}_0 = \mathbf{0}, \tag{2.15}$$

hence

$$\mathbf{r}_1 = (\gamma\mathbf{I} - \alpha\mathbf{A})^{-1}\mathbf{q}_0. \tag{2.16}$$

We also have

$$(\alpha\mathbf{A} + \mathbf{B})\mathbf{q}_1 = \mathbf{q}_0 - \gamma\mathbf{r}_1, \tag{2.17}$$

which, by the Fredholm Alternative Theorem, has a solution if and only if the right-hand side (RHS) is orthogonal to the vector $\mathbf{1}$ since the operator on the left hand side is a $\mathbb{W}$-matrix of deficiency one. This is immediately obvious since we know from (2.15) that $\mathbf{1}^{\mathrm{T}}\left((\alpha\mathbf{A} - \gamma\mathbf{I})\mathbf{r}_1 + \mathbf{q}_0\right) = 0$. Recognizing that $\mathbf{1}^{\mathrm{T}}\mathbf{A} = \mathbf{0}^{\mathrm{T}}$ since $\mathbf{A}$ is itself a $\mathbb{W}$-matrix gives the needed result.

We also see, by the same operation, that $\mathbf{1}^{\mathrm{T}}\mathbf{r}_1 = \frac{1}{\gamma}$, so we must impose $\mathbf{1}^{\mathrm{T}}\mathbf{q}_1 = -\frac{1}{\gamma}$. This condition combined with (2.17) uniquely defines $\mathbf{r}_1$.

We note, here, that this power series expansion is only valid in an appropriate range of parameters. To determine that range, we perform the following investigation.

The system is of the form

$$(\mathbf{M}_1 + \epsilon\mathbf{M}_2)\left(\sum_{i=0}^{\infty}\epsilon^i\mathbf{x}_i\right) = \mathbf{0}. \tag{2.18}$$

The matrix $\mathbf{M}_1 + \epsilon\mathbf{M}_2$ is a $\mathbb{W}$-matrix and is irreducible for all $\epsilon > 0$, evidenced by the fact that it has a unique stationary distribution, (2.9) and (2.10). Hence, for all

$\epsilon > 0$, the rank deficiency of $\mathbf{M}_1 + \epsilon \mathbf{M}_2$ is 1. The $\mathbf{x}_i$'s are uniquely determined as follows.

$$\mathbf{M}_1 \, \mathbf{x}_0 = \mathbf{0}, \tag{2.19}$$

however, the rank of $\mathbf{M}_1$ is not specified, so this equation alone does not determine $\mathbf{x}_0$. To do so, we must consider matching at the next order in ϵ. The equation is

$$\mathbf{M}_1 \, \mathbf{x}_1 = -\mathbf{M}_2 \, \mathbf{x}_0. \tag{2.20}$$

By the Fredholm Alternative Theorem, for there to be an $\mathbf{x}_1$ that satisfies this equation, the RHS must satisfy $\langle \mathbf{M}_2 \, \mathbf{x}_0, \mathbf{y} \rangle = 0$ for all $\mathbf{y}$ such that $\mathbf{M}_1^{\mathrm{T}} \mathbf{y} = \mathbf{0}$. If $\mathbf{M}_1$ and $\mathbf{M}_2$ are $n \times n$ and we define $k \leq n$ to be the rank of $\mathbf{M}_1$, then there are exactly $n - k$ linearly independent vectors $\mathbf{y}_1, \dots, \mathbf{y}_{n-k}$ which span the nullspace of $\mathbf{M}_1^{\mathrm{T}}$. One of these, say $\mathbf{y}_{n-k}$, is $\mathbf{1}^{\mathrm{T}}$. We know that $\mathbf{1}^{\mathrm{T}}$ is a left null vector for $\mathbf{M}_2$ because $\mathbf{M}_1 + \epsilon \mathbf{M}_2$ is a $\mathbb{W}$-matrix for all $\epsilon \geq 0$. In particular, it is a $\mathbb{W}$-matrix when $\epsilon = 0$. Hence, $\mathbf{M}_1$ is a $\mathbb{W}$-matrix. So, then

$$\mathbf{0} = \mathbf{1}^{\mathrm{T}} \left(\mathbf{M}_1 + \epsilon \mathbf{M}_2 \right) = \epsilon \, \mathbf{1}^{\mathrm{T}} \mathbf{M}_2 \quad \forall \, \epsilon > 0. \tag{2.21}$$

Now, define the $(n - k - 1) \times n$ matrix $\mathbf{Y}$ to have as its jth row $\mathbf{y}_j^{\mathrm{T}}$, $i = 1, \dots, n - k - 1$ and the $k \times n$ matrix $\widehat{\mathbf{M}}_1$ to have as its rows the k pivot rows of $\mathbf{M}_1$.

We now construct the $n \times n$ matrix

$$\mathbf{M} = \begin{pmatrix} \widehat{\mathbf{M}}_1 \\ \mathbf{Y} \, \mathbf{M}_2 \\ \mathbf{1}^{\mathrm{T}} \end{pmatrix} \tag{2.22}$$

and note that $\mathbf{M} \, \mathbf{x}_0 = \begin{pmatrix} \mathbf{0} \\ \mathbf{0} \\ 1 \end{pmatrix}$ of necessity.

We claim, without proof, that $\mathbf{M}$ is an invertible matrix. This is certainly not true in general, even for $\mathbf{M}_1 + \epsilon \mathbf{M}_2$ invertible. A counterexample is given by

$$\mathbf{M}_1 = \begin{pmatrix} 1 & 1 \\ 0 & 0 \end{pmatrix}, \quad \mathbf{M}_2 = \begin{pmatrix} 1 & 2 \\ 1 & 1 \end{pmatrix}. \tag{2.23}$$

Although, we believe it is true for irreducible $\mathbb{W}$-matrices, this remains to be proven. If this conjecture is true, however, it uniquely specifies $\mathbf{x}_0$.

Each of the $\mathbf{x}_i$'s for $i > 0$, then, satisfy

$$\mathbf{M}_1\,\mathbf{x}_i = -\mathbf{M}_2\,\mathbf{x}_{i-1}, \tag{2.24}$$

and, hence, must also satisfy

$$\mathbf{Y}\,\mathbf{M}_2\,\mathbf{x}_i = \mathbf{0}. \tag{2.25}$$

Furthermore, to ensure that $\sum \epsilon^i\,\mathbf{x}_i$ is a probability distribution for all ϵ, we must also enforce $\mathbf{1}^{\mathrm{T}}\,\mathbf{x}_i = \delta_{0,i}$. All of these conditions can be written succinctly as

$$\mathbf{M}\,\mathbf{x}_i = \mathbf{N}\,\mathbf{x}_{i-1}, \quad i = 1, 2, \ldots, \tag{2.26}$$

where

$$\mathbf{N} = \begin{pmatrix} -\widehat{\mathbf{I}}\,\mathbf{M}_2 \\ \mathbf{0} \\ \mathbf{0} \end{pmatrix}. \tag{2.27}$$

In other words,

$$\mathbf{x}_i = \mathbf{M}^{-1}\,\mathbf{N}\,\mathbf{x}_{i-1} = \left(\mathbf{M}^{-1}\,\mathbf{N}\right)^i \mathbf{x}_0. \tag{2.28}$$

Thus, in order for the power series to converge, we must choose ϵ small enough that

$$\frac{1}{\epsilon} > \max\left\{ |\lambda_k| \,\middle|\, \lambda_k \in \sigma\left(\mathbf{M}^{-1}\,\mathbf{N}\right) \right\}. \tag{2.29}$$

In the case of this first expansion, in the parameter β, the matrix $\mathbf{N}$ cannot have rank higher than the rank of $\begin{pmatrix} -\beta\mathbf{I} & \mathbf{0} \\ \beta\mathbf{I} & \mathbf{0} \end{pmatrix}$, which clearly has 0 as an eigenvalue with multiplicity $N + 1$. Computing the remaining eigenvalues of $\mathbf{M}^{-1}\,\mathbf{N}$ can be done without explicitly computing $\mathbf{M}^{-1}$, but does require the expansion of a determinant. If we choose $N \leq 4$, these eigenvalues can be computed by any symbolic math software. For large N, this computation becomes unwieldy. For small enough N, the nonzero eigenvalues are

$$\lambda_0 = -\frac{1}{\gamma}, \qquad \lambda_n = -\frac{\alpha}{(\alpha + 1)(\gamma + n\,\alpha)}, \quad n = 1, \ldots, N. \tag{2.30}$$

We suspect this holds for any positive integer N, but it remains to be proven. This gives us a tight bound for the convergence of our power series (2.11). With the stipulation that all parameters are positive, the series converges for all $\beta < \gamma$.

This distribution has the capacity to be bimodal, but appears to be so only for γ sufficiently less than α, though this range is difficult to quantify exactly. Figure

2.2 shows comparisons of truncations of the power series expansion (2.11) with data from Gillespie simulations. We see that for the parameter values chosen, we must plot several terms of the series in order for the truncation to be reasonably close to its limiting distribution. Also shown in the figure are the mean of the final truncation plotted and the equilibrium value predicted by the mean field model.

We observe that the probability of the process residing at states near the expected value or near the deterministic mean is relatively low in comparison with the peaks of the distribution. This is a case where modeling the reaction using the traditional mass-action kinetics may not be able to explain experimental results if such were to
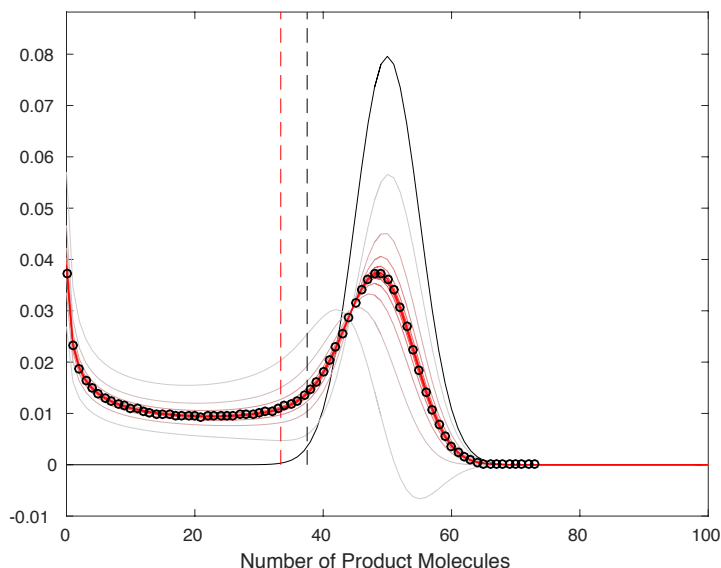
Figure 2.2. Expansion in β for simple enzymatic inhibition. The distribution of the number of product molecules in the system (2.2). Shown in the figure are: (1) the fraction of time spent in each state visited with a given number of product molecules during the course of a stochastic simulation using Gillespie's method (black data points). States without data points were not visited in the simulation, though there was a positive probability of doing so. (2) truncations of the power series expansion (2.11) which are shaded as curves that become increasingly more red as more terms are included. The first term $\mathbf{q}_0$ is plotted in black. For purposes of plotting only the distribution of product molecules, these curves are the sum of $\mathbf{p}_1$ and $\mathbf{p}_0$. They are discrete distributions, but are plotted as continuous curves here for visual contrast. (3) the mean of the final truncation plotted (vertical red dashed line). (4) the equilibrium value predicted by the deterministic and mean field models (vertical black dashed line). Parameter values are $\alpha = 1$, $\beta = 0.4$, $\gamma = 0.6$, $N = 100$, and $V = 1$.

give a high level of variability.

2.2.3.2   Expansion in γ

On the other hand, if instead we assume $\gamma \ll 1$ in (2.8) we can approximate the steady state as the power series in γ,

$$\begin{pmatrix} \mathbf{p}_1 \\ \mathbf{p}_0 \end{pmatrix} = \begin{pmatrix} \mathbf{u}_0 \\ \mathbf{v}_0 \end{pmatrix} + \gamma \begin{pmatrix} \mathbf{u}_1 \\ \mathbf{v}_1 \end{pmatrix} + O(\gamma^2). \tag{2.31}$$

Then, at $O(\gamma^0)$ we have the system,

$$(\alpha \mathbf{A} + \mathbf{B} - \beta \mathbf{I})\mathbf{u}_0 = \mathbf{0}$$
$$\beta \mathbf{u}_0 + \alpha \mathbf{A}\mathbf{v}_0 = \mathbf{0}. \tag{2.32}$$

Since $(\alpha \mathbf{A} + \mathbf{B} - \beta \mathbf{I})^\mathrm{T}$ is strictly diagonally dominant it is invertible, hence $\mathbf{u}_0 = \mathbf{0}$. Therefore $\mathbf{v}_0 = \mathbf{e}_0$. This makes sense as a first-order approximation, since if γ is small the enzyme spends most of its time in the inhibited state and all available P would convert to S and become depleted.

To get the $O(\gamma)$ correction we have the system

$$(\alpha \mathbf{A} + \mathbf{B} - \beta \mathbf{I})\mathbf{u}_1 + \mathbf{v}_0 = \mathbf{0}$$
$$\beta \mathbf{u}_1 + \alpha \mathbf{A}\mathbf{v}_1 - \mathbf{v}_0 = \mathbf{0}. \tag{2.33}$$

Hence,

$$\mathbf{u}_1 = -(\alpha \mathbf{A} + \mathbf{B} - \beta \mathbf{I})^{-1}\mathbf{v}_0, \tag{2.34}$$

and

$$\alpha \mathbf{A}\mathbf{v}_1 = \mathbf{v}_0 - \beta \mathbf{u}_1. \tag{2.35}$$

Again, this expansion is only valid for a particular range of γ. We notice that the nonzero eigenvalues of the relevant operator for this expansion are related to the eigenvalues in (2.30). It is easily shown that setting $\beta = \lambda_n^{-1}$ and solving for γ gives the multiplicative inverses of the eigenvalues for this expansion's operator. So, the eigenvalues of interest here are

$$\mu_0 = -\frac{1}{\beta}, \qquad \mu_n = -\frac{\alpha+1}{\alpha(\beta + n(\alpha+1))}, \quad n = 1, \ldots, N. \tag{2.36}$$

The remaining eigenvalues are, again, all 0. Therefore, with positive parameters, the series converges for $\gamma < \min\left\{\beta, \frac{\alpha(\beta+\alpha+1)}{\alpha+1}\right\}$.

Again, this distribution is bimodal for certain ranges of parameters. An example of such is shown in Figure 2.3. The bulk of this distribution remains in the first term of the power series expansion. One can clearly see the stationary probability of state 0 is much higher than any other state. However, there is a significant portion of the total probability mass over a range of other states. We observe that, again, the stationary probabilities near the expected value of this distribution are low. An expected value cannot adequately describe the important features of a bimodal distribution.

2.2.3.3 Expansion for large β, γ

Let ϵ be a small parameter such that $\frac{1}{\epsilon} = \beta + \gamma$, and let $\tilde{\beta} = \epsilon\beta$ and $\tilde{\gamma} = \epsilon\gamma$. Furthermore, we let the steady state solution be a power series in ϵ. Then we can rewrite (2.8) in steady state as

$$\mathbf{0} = \left(\frac{1}{\epsilon} \begin{pmatrix} -\tilde{\beta}\mathbf{I} & \tilde{\gamma}\mathbf{I} \\ \tilde{\beta}\mathbf{I} & -\tilde{\gamma}\mathbf{I} \end{pmatrix} + \begin{pmatrix} \alpha\mathbf{A} + \mathbf{B} & \\ & \alpha\mathbf{A} \end{pmatrix} \right) \left(\begin{pmatrix} \mathbf{x}_0 \\ \mathbf{y}_0 \end{pmatrix} + \epsilon \begin{pmatrix} \mathbf{x}_1 \\ \mathbf{y}_1 \end{pmatrix} + O(\epsilon^2) \right). \tag{2.37}$$

Then, the leading order equation tells us $\tilde{\beta}\mathbf{x}_0 = \tilde{\gamma}\mathbf{y}_0$.

Already, we suspect this distribution cannot be bimodal. The bimodality we have
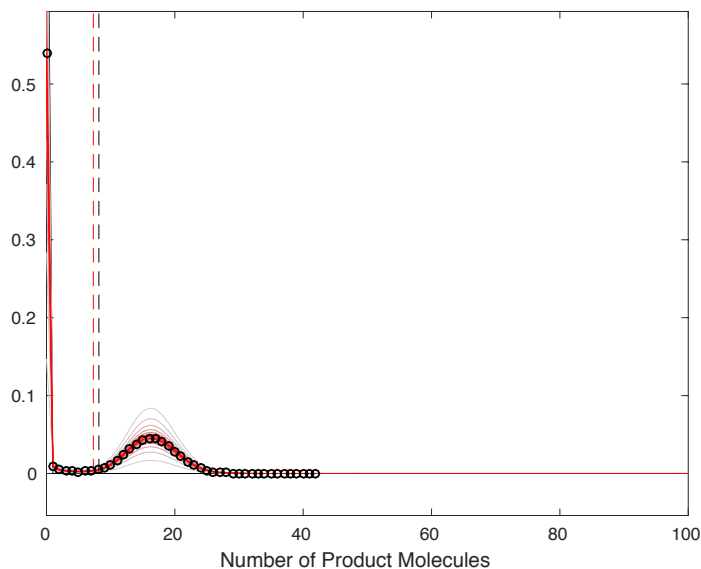
Figure 2.3. Expansion in γ for simple enzymatic inhibition. Objects plotted are the same as in Figure 2.2, but with respect to the expansion (2.31). Parameter values are $\alpha = 5$, $\beta = 0.1$, $\gamma = 0.08$, $N = 100$, and $V = 1$.

seen in the other distributions has come from a separation between the peaks of the $\mathbf{p}_1$ and $\mathbf{p}_0$ vectors. Here, since the leading order term of each is a multiple of the other, the peaks cannot be separated, and it is unlikely that one will be bimodal on its own, given the structure of the other matrices in the equation.

We must go to the next order in ϵ to learn more about the leading order term in (2.37). The next matching equations are

$$-\tilde{\beta}\mathbf{x}_1 + \tilde{\gamma}\mathbf{y}_1 + (\alpha\mathbf{A} + \mathbf{B})\mathbf{x}_0 = \mathbf{0},$$
$$\tilde{\beta}\mathbf{x}_1 - \tilde{\gamma}\mathbf{y}_1 + \alpha\mathbf{A}\mathbf{y}_0 = \mathbf{0},$$
(2.38)

which, when added together and $\frac{\tilde{\beta}}{\tilde{\gamma}}\mathbf{x}_0$ is substituted for $\mathbf{y}_0$, gives

$$\left(\frac{\alpha}{\tilde{\gamma}}\mathbf{A} + \mathbf{B}\right)\mathbf{x}_0 = \mathbf{0}.$$
(2.39)

Hence, $\mathbf{x}_0$, and, by extension, $\mathbf{y}_0$ are scaled binomial distributions with parameter $\frac{\tilde{\gamma}}{\tilde{\gamma}+\alpha}$. This parameter range does not yield a bimodal stationary distribution. For completeness we still include its radius of convergence. The nonzero eigenvalues of the operator as defined above are

$$\nu_n = -\frac{n\,\alpha(\alpha+1)}{\alpha+\tilde{\gamma}}, \quad n = 1, \ldots, N.$$
(2.40)

These eigenvalues increase in magnitude, rather than decrease, as a function of n, so the bound for convergence of this series is dependent on the relationship between γ, which we assume is large, and the system size: $\epsilon < \frac{\alpha}{N\,\alpha(\alpha+1)-\gamma}$ if $N\,\alpha(\alpha+1) > \gamma$. Otherwise, the series converges for all ϵ.

In this parameter regime the distributions (simulated and numerically computed) are unimodal and the prediction from the deterministic model lies almost exactly at the mean. This is a case where traditional deterministic modeling gives a good prediction of the behavior we expect from the stochastic system.

2.2.3.4   Some comments regarding the above expansions

The series in this section have been computed to lend some intuition about the shape of the stationary distribution of (2.8). This is not meant to be an exhaustive list of all possible parameter regimes. Rather, we choose the few examples given here to demonstrate that there are parameter ranges for which the process has a bimodal

stationary distribution and ranges for which its stationary distribution is unimodal. Another expansion that is clearly bimodal is the one obtained by assuming $\epsilon = \beta + \gamma$ is small. Its leading order term is the concatenation of the leading order terms we obtain in sections 2.2.3.1 and 2.2.3.2. These terms (and perhaps the leading order terms in all the expansions above) are not particularly surprising. They are merely the stationary distributions for when the enzyme is always, or, respectively, never active. The parameters we choose as small are the switching rates of the enzyme from active to inactive or vice versa, so, naturally, we expect the leading order terms to be as they are.

What is interesting about this model is that it stands in stark contrast to the deterministic and mean field models, neither of which has the capacity to predict bistable or bimodal behavior. Both of these models have a unique stable equilibrium point. In fact, they are equivalent models; only the variables have slightly different meanings. This contrast argues that for certain types of reactions the standard methods of modeling do not produce a full picture of the behavior of the system. Other modeling methods, such as the chemical master equation used here, are needed in order to help understand variability in reaction networks.

We now modify the chemical reaction system to have a negative feedback. Negative feedbacks often cause a system to have more stable behavior. We are interested to learn whether the negative feedback in the following examples removes the possibility of bimodality in the stochastic system.

2.3   Conserved Autoinhibition

The following is a different type of inhibition of the enzyme in the reaction, but retains a conservation property relating the amount of substrate and product in the system.

$$S + E \rightarrow E + P \rightleftarrows EI$$
$$P \rightarrow S. \tag{2.41}$$
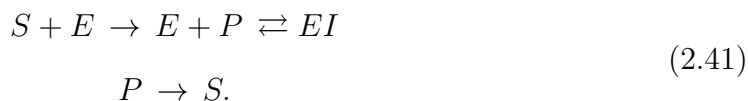
For consistency, we stay with the notation that EI is inhibited enzyme, though, in this reaction, we take it to denote the complex formed by enzyme binding to product. We consider this case to determine whether this different type of inhibition of the enzyme

affects the property seen in reaction (2.2), which is that the deterministic and mean field models cannot have multiple equilibria, but the stochastic master equation does have the possibility of a bimodal stationary distribution. It may be that inhibition of this form does allow for the deterministic model to exhibit multiple equilibria. Or it may be that autoinhibition of this form modifies the stationary distributions so as to eliminate the possibility of multimodality. As before, the deterministic and mean field models are equivalent. Hence, we need only consider one or the other here.

2.3.1   Mean Field Model

The equations for the mean field model describing reaction (2.41) are

$$\dot{c}_S = -k_{E+S \to E+P}\, p_A\, c_S + k_{P \to S}\, c_P,$$
$$\dot{p}_A = -k_{E+P \to EI}\, p_A\, c_P + k_{EI \to E+P}\, (1 - p_A),$$

(2.42)

with

$$\dot{c}_P = -\dot{c}_S + \dot{p}_A.$$

(2.43)

This gives the conservation law $c_{S_T} = c_P + c_S - p_A$. Here, c_{S_T} is not actually a concentration, but, since it is a constant in this system, we use the same notation as above. In equilibrium

$$p_A = \frac{k_{EI \to E+P}}{k_{E+P \to EI}\, c_P + k_{EI \to E+P}}.$$

(2.44)

Substituting this and our conservation law into the equilibrium equation for c_P yields the cubic polynomial equation

$$0 = k_3\, c_p^3 + k_2\, c_p^2 + k_1\, c_p + k_0,$$

(2.45)

where

$$k_3 = -k_{E+P \to EI}^2\, k_{P \to S},$$
$$k_2 = -k_{E+P \to EI}\, k_{EI \to E+P}\, (k_{E+S \to E+P} + 2\, k_{P \to S}),$$
$$k_1 = k_{E+S \to E+P}\, k_{E+P \to EI}\, k_{EI \to E+P}\, c_{S_T} - k_{EI \to E+P}^2\, (k_{P \to S} + k_{E+S \to E+P}),$$
$$k_0 = k_{E+S \to E+P}\, k_{EI \to E+P}^2\, (c_{S_T} + 1).$$

(2.46)

We notice that $k_3, k_2 < 0$ for any set of positive rate constants. We also observe that $k_0 > 0$ since $c_{S_T} > -1$. The sign of k_1 may be positive or negative depending on the reaction rates, but either way there is exactly one change of sign of coefficients in the

polynomial (2.45), that between k_2 and k_1 or between k_1 and k_0. So, by Descartes' rule of signs, (2.45) has exactly one positive root c_p^*.

This model, and, by extension, the deterministic model from the law of mass action, can only admit one positive equilibrium for any set of positive rate constants. Since we have already shown the existence of a positive finitely bounded invariant region, and since the system is only two-dimensional, this equilibrium must be stable. As with the first reaction system, we contrast this model's results with possible equilibria derived from the discrete stochastic model.

2.3.2 Stochastic Model

Due to the similarities between this reaction network and (2.2) we write the nondimensionalized master equation using similar notation.

$$\frac{d}{d\tau}\begin{pmatrix} \mathbf{p}_1 \\ \mathbf{p}_0 \end{pmatrix} = \begin{pmatrix} \alpha\mathbf{A}_N + \mathbf{B}_N - \beta\mathbf{C}_N & \begin{pmatrix} 0 & \cdots & 0 \\ & \gamma\mathbf{I}_{N-1} & \end{pmatrix} \\ \beta\widetilde{\mathbf{C}_N} & \alpha\mathbf{A}_{N-1} - \gamma\mathbf{I}_{N-1} \end{pmatrix}\begin{pmatrix} \mathbf{p}_1 \\ \mathbf{p}_0 \end{pmatrix} \qquad (2.47)$$

where subscripts, j on matrices denote that they are square, $(j+1) \times (j+1)$ with indices $0, \ldots, j$, and the tilde above denotes the deletion of the first row. Thus, $\widetilde{\mathbf{C}_N}$ is, in fact, $N \times (N+1)$, once we define

$$\mathbf{C} = \begin{pmatrix} 0 & & & \\ & 1 & & \\ & & \ddots & \\ & & & N \end{pmatrix}. \qquad (2.48)$$

The matrix in (2.47) is pieced together in such a conglomerated fashion because the number of possible P molecules depends on whether one molecule is bound to, and inhibiting, the enzyme molecule in the system. As a consequence, $\mathbf{p}_1$ remains as defined in (2.7), but $\mathbf{p}_0 = \begin{pmatrix} p_{0,0} & \cdots & p_{N-1,0} \end{pmatrix}^{\mathrm{T}}$.

We now approximate the stationary distribution for this process by using power series in certain parameter ranges as above. Here we only choose parameter ranges that give "interesting" or bimodal behavior in the first reaction scheme.

2.3.2.1 Expansion in β

Using our redefined notation we write the first power series approximation

$$\begin{pmatrix} \mathbf{p}_1 \\ \mathbf{p}_0 \end{pmatrix} = \begin{pmatrix} \mathbf{q}_0 \\ \mathbf{r}_0 \end{pmatrix} + \beta\begin{pmatrix} \mathbf{q}_1 \\ \mathbf{r}_1 \end{pmatrix} + O(\beta^2). \qquad (2.49)$$

Matching terms in β gives the first matching condition

$$\left(\alpha \mathbf{A}_{N-1} - \gamma \mathbf{I}_{N-1}\right) \mathbf{r}_0 = \mathbf{0}. \tag{2.50}$$

Since this matrix is invertible for all nonzero γ we see $\mathbf{r}_0 = \mathbf{0}$. So, then,

$$\left(\alpha \mathbf{A}_N + \mathbf{B}_N\right) \mathbf{q}_0 = \mathbf{0}. \tag{2.51}$$

Once again, $\mathbf{q}_0$ is binomially distributed with parameter $\frac{1}{1+\alpha}$. It makes sense that this distribution would be the same as (2.14), because it is the leading order approximation for the distribution when the enzyme is active. However, the first order correction term is slightly different. It is

$$\mathbf{r}_1 = \left(\gamma \mathbf{I}_{N-1} - \alpha \mathbf{A}_{N-1}\right)^{-1} \widetilde{\mathbf{C}_N} \, \mathbf{q}_0. \tag{2.52}$$

Comparing this to the correction term in (2.16) shows their obvious similarity. The vector $\mathbf{q}_1$ is obtained by, once again, enforcing the condition $\mathbf{1}^{\mathrm{T}} \begin{pmatrix} \mathbf{q}_1 \\ \mathbf{r}_1 \end{pmatrix} = 0$. In this way all further terms in the series can be computed. An example of a bimodal distribution given by this expansion is seen in Figure 2.4. Again, this expansion is only valid for a certain range of β, however the eigenvalues of this matrix are not so easily guessed. We rely on the numerical solutions to indicate whether the series converges or diverges. The bound on β appears to be much tighter than that for (2.11).

2.3.2.2 Expansion in γ

As we see above, the other parameter regime that yields a possible bimodal distribution is when γ is sufficiently small. Here, we use the same series expansion,

$$\begin{pmatrix} \mathbf{p}_1 \\ \mathbf{p}_0 \end{pmatrix} = \begin{pmatrix} \mathbf{u}_0 \\ \mathbf{v}_0 \end{pmatrix} + \gamma \begin{pmatrix} \mathbf{u}_1 \\ \mathbf{v}_1 \end{pmatrix} + O(\gamma^2). \tag{2.53}$$

Then, at leading order

$$\left(\alpha \mathbf{A}_N + \mathbf{B}_N - \beta \mathbf{C}_N\right) \mathbf{u}_0 = \mathbf{0}. \tag{2.54}$$

The matrix on the LHS of this equation is invertible. The proof of this, due to Earnshaw and Keener [4], is as follows. We make use of the fact that $\alpha \mathbf{A}_N + \mathbf{B}_N$ is an irreducible $\mathbb{W}$-matrix and that $\beta \mathbf{C}_N$ is a nonzero, nonnegative, diagonal matrix.
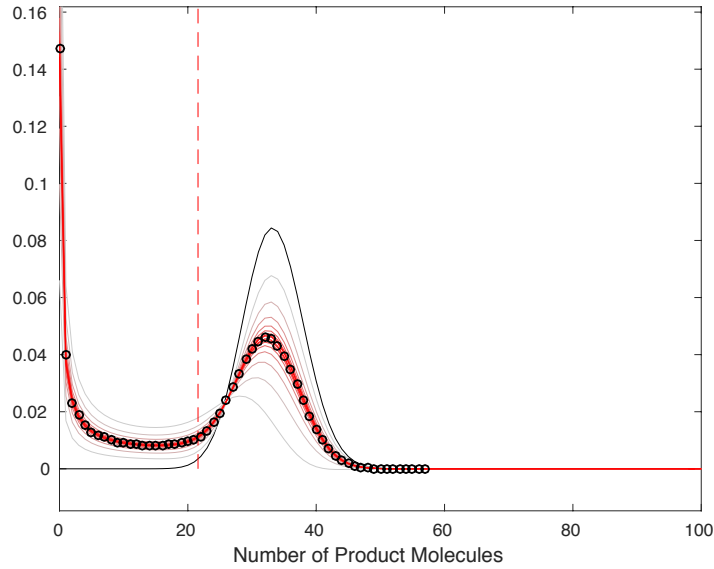
Figure 2.4. Expansion in β for conserved enzymatic autoinhibition. Similar to previous figures. Corresponds to (2.49). Mean field equilibrium point is not shown. Parameter values are $\alpha = 2$, $\beta = 0.01$, $\gamma = 0.5$, $N = 100$, and $V = 1$.

Hence, there exists a $\zeta > 0$ large enough that $\mathbf{G} = \alpha \mathbf{A}_N + \mathbf{B}_N - \beta \mathbf{C}_N + \zeta \mathbf{I}_N$ is a nonnegative irreducible matrix. Then, by the Perron-Frobenius Theorem, $\mathbf{G}$ has a unique positive eigenvector $\mathbf{w}$ whose corresponding eigenvalue r is real and is the spectral radius of $\mathbf{G}$. So, then,

$$r\mathbf{w} = \mathbf{G}\mathbf{w} = \left(\alpha \mathbf{A}_N + \mathbf{B}_N - \beta \mathbf{C}_N + \zeta \mathbf{I}_N\right) \mathbf{w}, \tag{2.55}$$

which, with a little manipulation, yields the inequality

$$r - \zeta = \frac{-\beta \, \mathbf{1}^{\mathrm{T}} \mathbf{C}_N \mathbf{w}}{\mathbf{1}^{\mathrm{T}} \mathbf{w}} < 0. \tag{2.56}$$

Since all eigenvalues of $\mathbf{G}$ are contained in a disc of radius r centered at the origin, eigenvalues of $\alpha \mathbf{A}_N + \mathbf{B}_N - \beta \mathbf{C}_N$ are contained in a disc of the same radius centered at $-\zeta$. Since $r < \zeta$, we see that 0 is not an eigenvalue of this matrix.

It follows that $\mathbf{u}_0 = \mathbf{0}$, and, hence,

$$\alpha \mathbf{A}_{N-1} \mathbf{v}_0 = \mathbf{0} \implies \mathbf{v}_0 = \mathbf{e}_0. \tag{2.57}$$

We get the first order correction from the equation

$$\left(\alpha \mathbf{A}_N + \mathbf{B}_N - \beta \mathbf{C}_N\right) \mathbf{u}_1 + \begin{pmatrix} 0 & \cdots & 0 \\ & \mathbf{I}_{N-1} & \end{pmatrix} \mathbf{v}_0 = \mathbf{0}, \tag{2.58}$$

whence comes

$$\mathbf{u}_1 = -\left(\alpha \mathbf{A}_N + \mathbf{B}_N - \beta \mathbf{C}_N\right)^{-1} \begin{pmatrix} 0 \\ \mathbf{v}_0 \end{pmatrix}. \tag{2.59}$$

This distribution only looks slightly different than the distribution in Figure 2.3. There exist parameters for which it is bimodal.

2.4   Nonconserved Autoinhibition

Now we modify the autoinhibition reaction further. This reaction system does not have the same type of conservation law as we see in the others, but we can investigate it in a similar fashion.

$$\begin{aligned} E &\to E + P \rightleftarrows EI \\ P &\to \emptyset. \end{aligned} \tag{2.60}$$

This reaction can be thought of in a few different ways. One of these ways is that the "enzyme," E can be thought of as a catalyst acting on a reservoir of substrate so large that its change is negligible. Hence, the "substrate" concentration (if there is such) can be absorbed into the rate constant representing production of product. Alternatively, the reaction can be thought of as a gene, either on DNA or RNA, that transcribes some product, P. P may be a protein or RNA itself. Either way, P can then bind to the gene and inhibit its own production. Clearly the reaction (2.60) is a very simplified version of either of these interpretations, but it serves to illustrate the features we wish to observe.

Again, we make a brief investigation of the mean field (and, by extension, the deterministic) model to analyze its long-term or steady state behavior.

2.4.1   Mean Field Model

As is our pattern, let p_A be the probability that the enzyme is in its active state and c_P be the concentration of product molecules, P. We obtain the mean field model

$$\begin{aligned} \dot{p}_A &= -k_{E+P \to EI}\, c_P\, p_A + k_{EI \to E+P}\, (1 - p_A) \\ \dot{c}_P &= k_{E \to E+P}\, p_A - k_{P \to \emptyset}\, c_P + \dot{p}_A. \end{aligned} \tag{2.61}$$

In steady state, this model yields the quadratic equation

$$q(c_P) = -k_{E+P \to EI}\, k_{P \to \emptyset}\, c_P^2 - k_{EI \to E+P}\, k_{P \to \emptyset}\, c_P + k_{E \to E+P}\, k_{EI \to E+P} = 0. \tag{2.62}$$

Since $q(0) > 0$ and $q''(0) < 0$ this equation has exactly one positive root c_P^*. And, in steady state, $p_A^* = \frac{k_{P \to \emptyset} c_P^*}{k_{E \to E+P}}$. This equilibrium is clearly stable since the trace of the Jacobian is negative and the determinant is positive for all positive values of p_A and c_P. This holds for all positive rate constants. Hence, there is no way this model can produce multiple nonnegative equilibria.

2.4.2 Stochastic Model

For ease of notation, we nondimensionalize so that $\alpha = k_{E \to E+P}/k_{P \to \emptyset}$, $\beta = k_{E+P \to EI}/k_{P \to \emptyset}$, and $\gamma = k_{EI \to E+P}/k_{P \to \emptyset}$. We have scaled by the rate of degradation of P rather than its rate of production simply to make the calculations less messy-looking. We can still relate the following results to our results above because none of our expansions are in the parameter α. The nondimensionalized master equation for this reaction, then, is

$$\frac{d}{d\tau}\begin{pmatrix} \mathbf{p}_1 \\ \mathbf{p}_0 \end{pmatrix} = \begin{pmatrix} \alpha\mathbf{A} + \mathbf{B} - \beta\mathbf{C} & \begin{pmatrix} 0 & \cdots \\ & \gamma\mathbf{I} \end{pmatrix} \\ \beta\widetilde{\mathbf{C}} & \mathbf{B} - \gamma\mathbf{I} \end{pmatrix}\begin{pmatrix} \mathbf{p}_1 \\ \mathbf{p}_0 \end{pmatrix}, \tag{2.63}$$

where $\mathbf{p}_1$ is the "vector" of probabilities that the number of product molecules P in solution is $n_P = 0, 1, 2, \ldots$ and the enzyme is active, or unbound, to a product molecule. Similarly, $\mathbf{p}_0$ is the "vector" of probabilities for n_P while the enzyme is inhibited by a product molecule. The product molecule bound to the enzyme is not included in the count n_P. The reason for the quotation marks around the word "vector" is that these are really sequences in ℓ^1. The operators $\mathbf{A}$, $\mathbf{B}$, $\mathbf{C}$, $\widetilde{\mathbf{C}}$, and $\mathbf{I}$ are not matrices, but are operators on ℓ^1. Their structure is as follows:

$$\mathbf{A} = \begin{pmatrix} -1 & & & \\ 1 & -1 & & \\ & 1 & -1 & \\ & & \ddots & \ddots \end{pmatrix}, \tag{2.64}$$

$$\mathbf{B} = \begin{pmatrix} 0 & 1 & & \\ & -1 & 2 & \\ & & -2 & 3 \\ & & & \ddots & \ddots \end{pmatrix}, \tag{2.65}$$

$$\mathbf{C} = \begin{pmatrix} 0 & & & \\ & 1 & & \\ & & 2 & \\ & & & \ddots \end{pmatrix}, \tag{2.66}$$

$\widetilde{\mathbf{C}}$ is merely $\mathbf{C}$ with the first row deleted, and $\mathbf{I}$ is the identity operator.

We consider this master equation in steady state. Since solving it analytically doesn't seem to give much intuition about the shape of the distribution we try a few power expansions in various parameter regimes.

2.4.2.1 Expansion in β

If β is a small enough parameter that we can expand the solution as a series in β, then the governing equation in steady state is

$$\mathbf{0} = \left(\left(\begin{pmatrix} \alpha\mathbf{A} + \mathbf{B} & \begin{pmatrix} 0 & \cdots \\ & \gamma\mathbf{I} \end{pmatrix} \\ \mathbf{0} & \mathbf{B} - \gamma\mathbf{I} \end{pmatrix} \right) + \beta \begin{pmatrix} \mathbf{C} & \mathbf{0} \\ \widetilde{\mathbf{C}} & \mathbf{0} \end{pmatrix} \right) \left(\begin{pmatrix} \mathbf{x}_0 \\ \mathbf{y}_0 \end{pmatrix} + \beta \begin{pmatrix} \mathbf{x}_1 \\ \mathbf{y}_1 \end{pmatrix} + O(\beta^2) \right). \tag{2.67}$$

The leading order equation,

$$(\mathbf{B} - \gamma\mathbf{I})\, \mathbf{y}_0 = \mathbf{0}, \tag{2.68}$$

tells us that $\mathbf{y}_0 = \mathbf{0}$. The operator $\mathbf{B} - \gamma\mathbf{I}$ does, in fact, have a nontrivial null vector, but it is not in ℓ^1. It has the character that $y_{0,n+1} = \frac{\gamma+n}{1+n}\, y_{0,n}$. The ratio test is inconclusive for this series, but its lack of convergence can be shown using Raabe's test. This test asserts that if

$$\lim_{n\to\infty} \left| \frac{y_n}{y_{n+1}} \right| = 1, \tag{2.69}$$

and

$$\lim_{n\to\infty} n \left(\left| \frac{y_n}{y_{n+1}} \right| - 1 \right) = \rho, \tag{2.70}$$

then the series is absolutely convergent if $\rho > 1$ and divergent if $\rho < 1$. In this case $\rho = 1 - \gamma < 1$. We make use of this nullspace later in this calculation.

The other leading order equation, then, becomes

$$(\alpha\mathbf{A} + \mathbf{B})\, \mathbf{x}_0 = \mathbf{0}. \tag{2.71}$$

Hence, $\mathbf{x}_0$ is Poisson with parameter α: $x_{0,n} = \dfrac{\alpha^n}{e^\alpha n!}$.

The equation for the first order correction to this steady state approximation is

$$(\mathbf{B} - \gamma \mathbf{I}) \, \mathbf{y}_1 = -\widetilde{\mathbf{C}} \, \mathbf{x}_0. \tag{2.72}$$

Using substitution, it is straightforward to show that a particular solution to this equation is

$$y_n = \frac{-1}{e^{-\alpha} n!} \left(\sum_{i=0}^{n} \alpha^i \prod_{j=i}^{n-1} (\gamma + j) \right), \tag{2.73}$$

where empty products are 1. However, this solution is not in ℓ^1 nor are any of its entries positive. All terms in the power series must be ℓ^1, and this particular term must have all positive entries since it is the first nonzero term for $\mathbf{p}_0$. To find a solution that is ℓ^1 we add the appropriate multiple of the null vector $z_n = \frac{1}{n!} \prod_{j=0}^{n-1} (\gamma + j)$. In order to have any hope of this approach yielding a useful result, at bare minimum we must choose z so that

$$\lim_{n \to \infty} y_n = \lim_{n \to \infty} \frac{z}{n!} \prod_{j=0}^{n-1} (\gamma + j) - \frac{1}{e^{\alpha} \, n!} \left(\sum_{i=0}^{n} \alpha^i \prod_{j=i}^{n-1} (\gamma + j) \right) = 0. \tag{2.74}$$

Rewriting in a simpler form,

$$y_n = \frac{1}{n!} \prod_{j=0}^{n-1} (\gamma + j) \left(z - e^{-\alpha} \sum_{i=0}^{n} \alpha^i \prod_{j=0}^{i-1} \frac{1}{\gamma + j} \right). \tag{2.75}$$

The term with the series in parentheses converges to a finite limit as $n \to \infty$. We let z be this limit and now define

$$\begin{aligned}
y_{1,n} &= \frac{1}{e^{\alpha} \, n!} \prod_{j=0}^{n-1} (\gamma + j) \left(\sum_{i=n+1}^{\infty} \alpha^i \prod_{j=0}^{i-1} \frac{1}{\gamma + j} \right) \\
&= \frac{\Gamma(\gamma + n)}{e^{\alpha} \, n!} \left(\sum_{i=n+1}^{\infty} \frac{\alpha^i}{\Gamma(\gamma + i)} \right).
\end{aligned} \tag{2.76}$$

Each entry of this vector is positive, as we hoped. Now we must show that $\sum_n y_{1,n} < \infty$. To this end we apply the ratio test.

$$\lim_{n\to\infty}\left|\frac{y_{1,n-1}}{y_{1,n}}\right| = \lim_{n\to\infty}\left(\frac{n}{n+\gamma-1}\right)\left(\frac{\frac{\alpha^n}{\Gamma(\gamma+n)}+\sum_{i=n+1}^{\infty}\frac{\alpha^i}{\Gamma(\gamma+i)}}{\sum_{i=n+1}^{\infty}\frac{\alpha^i}{\Gamma(\gamma+i)}}\right) \qquad (2.77)$$

$$= \lim_{n\to\infty}\left(\frac{n}{n+\gamma-1}\right)\left(\frac{1}{\sum_{i=n+1}^{\infty}\alpha^{i-n}\frac{\Gamma(\gamma+n)}{\Gamma(\gamma+i)}}+1\right) \qquad (2.78)$$

$$= \lim_{n\to\infty}\left(\frac{n}{n+\gamma-1}\right)\left(\frac{1}{\sum_{j=1}^{\infty}\alpha^{j}\frac{\Gamma(\gamma+n)}{\Gamma(\gamma+n+j)}}+1\right) \qquad (2.79)$$

$$= \lim_{n\to\infty}\left(\frac{n}{n+\gamma-1}\right)\left(\frac{1}{\sum_{j=1}^{\infty}\alpha^{j}\prod_{k=0}^{j-1}\frac{1}{\gamma+n+k}}+1\right) \qquad (2.80)$$

$$\geq \lim_{n\to\infty}\left(\frac{n}{n+\gamma-1}\right)\left(\frac{1}{\sum_{j=1}^{\infty}\alpha^{j}\frac{1}{(\gamma+n)^j}}+1\right) \qquad (2.81)$$

$$= \lim_{n\to\infty}\left(\frac{n}{n+\gamma-1}\right)\left(\frac{n+\gamma}{\alpha}\right) \qquad (2.82)$$

$$= \infty. \qquad (2.83)$$

To show convergence we merely need $\lim_{n\to\infty}\left|\frac{y_{1,n-1}}{y_{1,n}}\right| > 1$. However, since this limit is, in fact, ∞, this series appears to converge quite rapidly. It is not a long-tailed distribution. The remaining piece of this vector, $\mathbf{x}_1$ satisfies the equation

$$(\alpha\mathbf{A}+\mathbf{B})\,\mathbf{x}_1 = -\begin{pmatrix} 0 & \cdots \\ & \gamma\mathbf{I} \end{pmatrix}\mathbf{y}_1 - \mathbf{C}\mathbf{x}_0 \qquad (2.84)$$

whose terms are not easily guessed. Further terms in this series may be impossible to compute analytically, but these first two, at least, indicate that the bulk of the distribution lies within some finite range. This is useful for plotting, since we can't very well ask a computer to solve an infinite matrix equation. We can, however, truncate the state space, and, hence, the $\mathbb{W}$-matrix, by choosing N large enough that the total probability mass for all $n > N$ is within machine precision.

From numerical experiments, the bound on β for which this series converges appears to be even more restricted than the aforementioned examples. For instance, Figure 2.5 shows bimodal distributions for the parameters $\alpha = 30$, $\beta = 0.01$, and $\gamma = 0.5$. With this set of parameters we do see convergence. However, increasing α to 40 produces a power series that appears to diverge. The stochastic simulations still produce bimodal time distributions for these parameters, though it is unclear what, if any, expansion might give intuition about the reaction.
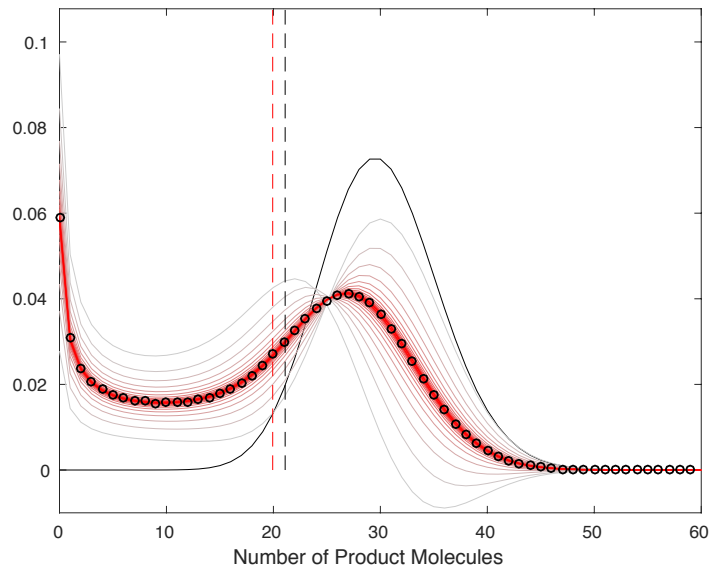
Figure 2.5. Expansion in β for nonconserved enzymatic autoinhibition. Similar to previous figures. Corresponds to the expansion in (2.67). Parameter values are $\alpha = 30$, $\beta = 0.01$, $\gamma = 0.5$, and $V = 1$. The system has been truncated to $N = 60$ without losing any visible fidelity.

2.4.2.2 Expansion in γ

For completeness, we now treat γ as the small parameter in the system and represent the solution as the power series

$$\begin{pmatrix} \mathbf{p}_1 \\ \mathbf{p}_0 \end{pmatrix} = \begin{pmatrix} \mathbf{x}_0 \\ \mathbf{y}_0 \end{pmatrix} + \gamma \begin{pmatrix} \mathbf{x}_1 \\ \mathbf{y}_1 \end{pmatrix} + O(\gamma^2). \tag{2.85}$$

Then, the first leading order equation is

$$\left(\alpha \mathbf{A} + \mathbf{B} - \beta \mathbf{C}\right) \mathbf{x}_0 = \mathbf{0}. \tag{2.86}$$

We claim that this equation implies that $\mathbf{x}_0 = \mathbf{0}$. The operator $\alpha \mathbf{A} + \mathbf{B} - \beta \mathbf{C}$ does appear to have a nontrivial null vector, but its form is not evident. In order for it to make sense in our solution expansion (2.85) it must be nonnegative. From the 0th row of (2.86), we get the condition

$$x_{0,1} = \alpha \, x_{0,0}. \tag{2.87}$$

All other rows can be written

$$\alpha x_{0,n} - (\alpha + (n+1)(1+\beta)) \, x_{0,n+1} + (n+2)x_{0,n+2} = 0. \tag{2.88}$$

We now define the generating function $G(z) = \sum_{n=0}^{\infty} x_{0,n} z^n$. Multiplying each row (2.88) by z^n and summing yields

$$
\begin{aligned}
0 &= \alpha \sum_{n=0}^{\infty} x_{0,n} z^n - \alpha z^{-1} \sum_{n=0}^{\infty} x_{0,n+1} z^{n+1} - (1+\beta) \sum_{n=0}^{\infty} x_{0,n+1} (n+1) z^n \\
&\quad + \sum_{n=0}^{\infty} x_{0,n+2} (n+1) z^n + \sum_{n=0}^{\infty} x_{0,n+2} z^n
\end{aligned}
\tag{2.89}
$$

$$
\begin{aligned}
&= \alpha\, G(z) - \alpha\, z^{-1} \left(G(z) - x_{0,0} \right) - (1+\beta) \sum_{n=0}^{\infty} x_{0,n+1} \frac{d}{dz} z^{n+1} \\
&\quad + \sum_{n=0}^{\infty} x_{0,n+2} \frac{d}{dz} z^{n+1} + z^{-2} \sum_{n=0}^{\infty} x_{0,n+2} z^{n+2}
\end{aligned}
\tag{2.90}
$$

$$
\begin{aligned}
&= \alpha \left(1 - z^{-1} \right) G(z) + \alpha\, z^{-1} x_{0,0} - (1+\beta) \frac{d}{dz} \left(\sum_{n=0}^{\infty} x_{0,n} z^n - x_{0,0} \right) \\
&\quad + \frac{d}{dz} \left(z^{-1} \sum_{n=0}^{\infty} x_{0,n+2} z^{n+2} \right) + z^{-2} \left(\sum_{n=0}^{\infty} x_{0,n} z^n - x_{0,1} z - x_{0,0} \right)
\end{aligned}
\tag{2.91}
$$

$$
\begin{aligned}
&= \alpha \left(1 - z^{-1} \right) G(z) + \alpha\, z^{-1} x_{0,0} - (1+\beta) \frac{dG}{dz} \\
&\quad + \frac{d}{dz} \left(z^{-1} \left(G(z) - x_{0,1} z - x_{0,0} \right) \right) + z^{-2} \left(G(z) - x_{0,1} z - x_{0,0} \right)
\end{aligned}
\tag{2.92}
$$

$$
= \alpha \left(1 - z^{-1} \right) G(z) + \alpha\, z^{-1} x_{0,0} - (1+\beta) \frac{dG}{dz} + z^{-1} \left(\frac{dG}{dz} - x_{0,1} \right).
\tag{2.93}
$$

Applying condition (2.87) and multiplying by z yields a homogeneous, linear, first-order ODE for $G(z)$,

$$
0 = (1 - (1+\beta) z) \frac{dG}{dz} + \alpha\, (z-1)\, G(z).
\tag{2.94}
$$

It is clear from (2.94) that $\frac{dG}{dz}\big|_{z=1} = 0$. Additionally, we know that $G(1) = \sum_{n=0}^{\infty} x_{0,n}$. If $x_{0,n} \geq 0$ for all n, as must be the case for our series expansion, then it follows that $G(1) \geq 0$ and $G(z) \leq G(1)$ for all $0 \leq z < 1$. However, differentiating (2.94) yields

$$
0 = -(1+\beta) \frac{dG}{dz} + (1 - (1+\beta) z) \frac{d^2 G}{dz^2} + \alpha\, G(z) + \alpha\, (z-1) \frac{dG}{dz},
\tag{2.95}
$$

which, when evaluated at $z = 1$ gives

$$
\frac{d^2 G}{dz^2}\bigg|_{z=1} = \frac{\alpha}{\beta}\, G(1).
\tag{2.96}
$$

If $G(1) = 0$, then $x_{0,n} = 0$ for all n. If, instead, $G(1) > 0$, then (2.96) tells us there is a $0 < z^* < 1$ for which $G(z^*) > G(1)$. This is not possible and provides a contradiction. Therefore, it must be that $\mathbf{x}_0 = \mathbf{0}$.

The leading-order term in our expansion, then, must satisfy

$$\mathbf{B}\,\mathbf{y}_0 = \mathbf{0}. \tag{2.97}$$

Resultantly, $\mathbf{y}_0 = \mathbf{e}_0$, the distribution with no product molecules, since the unbinding of the inhibited enzyme is slow compared to the degradation of P.

The first-order correction equations are

$$(\alpha\mathbf{A} + \mathbf{B} - \beta\mathbf{C})\,\mathbf{x}_1 + \begin{pmatrix} 0 & \cdots \\ & \gamma\mathbf{I} \end{pmatrix}\mathbf{y}_0 = \mathbf{0},$$

$$\widetilde{\mathbf{C}}\,\mathbf{x}_1 + \mathbf{B}\,\mathbf{y}_1 - \mathbf{I}\,\mathbf{y}_0 = \mathbf{0}. \tag{2.98}$$

Analytical solutions for these are not readily found, nor do these equations provide much insight into how further terms in the expansion modify its shape.

2.5   Discussion

The chemical reactions discussed in this chapter are all very similar. Indeed, a glance at Figures 2.2, 2.4, and 2.5 may lead one to believe that they are the exact same reaction. However, we have included each of these examples in a sequence that leads from a toy model toward a more realistic reaction that may be found in a biological or chemical system. The purpose of the toy model, reaction (2.2), is to gain intuition about the underlying probability distributions. We can see that these distributions remain consistent in character, even as we add complexity to the reaction and the resulting chemical master equation.

The main purpose of this analysis is to demonstrate that great caution is needed when mathematically modeling even the simplest of chemical reactions. Analytical results abound for deterministic ordinary differential equation systems obtained by the law of mass action, though there remain many unanswered questions about such systems. We show, in this chapter, that for certain reactions those analytical results do not predict even the most fundamental characteristics of the distributions we might expect to see in laboratory experiments.

2.6   References

[1] G. Craciun and M. Feinberg, *Multiple equilibria in the complex chemical reaction networks: I. The injectivity property*, SIAM J. Appl. Math., 65 (2005), pp. 1526–1546.

[2] ——, *Multiple equilibria in the complex chemical reaction networks: II. The species-reaction graph*, SIAM J. Appl. Math., 66 (2006), pp. 1321–1338.

[3] G. Craciun, Y. Tang, and M. Feinberg, *Understanding bistability in complex enzyme-driven reaction networks*, PNAS, 103 (2006), pp. 8697–8702.

[4] B. A. Earnshaw and J. P. Keener, *Global asymptotic stability of solutions of nonautonomous master equations*, SIAM J. Appl. Dyn. Syst., 9 (2010), pp. 220–237.

[5] A. Goldbeter and D. E. Koshland, Jr., *An amplified sensitivity arising from covalent modification in biological systems*, PNAS, 78 (1981), pp. 6840–6844.

[6] L. Michaelis and M. L. Menten, *Die kinetik der invertinwirkung*, Biochemische Zeitschrift, 49 (1913), pp. 333–369.

[7] C. A. Miller and D. A. Beard, *The effects of reversibility and noise on stochastic phosphorylation cycles and cascades*, Biophys. J., 95 (2008), pp. 2183–2192.

[8] M. Samoilov, S. Plyasunov, and A. P. Arkin, *Stochastic amplification and signaling in enzymatic futile cycles through noise-induced bistability with oscillations*, PNAS, 102 (2005), pp. 2310–2315.

CHAPTER 3

SLOW MANIFOLD REDUCTION OF A STOCHASTIC CHEMICAL REACTION: EXPLORING KEIZER'S PARADOX

SLOW MANIFOLD REDUCTION OF A STOCHASTIC CHEMICAL REACTION: EXPLORING KEIZER'S PARADOX

Parker Childs and James P. Keener

Department of Mathematics
University of Utah
Salt Lake City, UT 84112, USA

Dedicated to Professor Avner Friedman on the occasion of his 80th birthday. Congratulations, Avner, on your far too many to mention accomplishments!

Abstract. Keizer's paradox refers to the observation that deterministic and stochastic descriptions of chemical reactions can predict vastly different long term outcomes. In this paper, we use slow manifold analysis to help resolve this paradox for four variants of a simple autocatalytic reaction. We also provide rigorous estimates of the spectral gap of important linear operators, which establishes parameter ranges in which the slow manifold analysis is appropriate.

1. **Introduction.** In 1987, Joel Keizer proposed a simple autocatalytic chemical reaction for which the deterministic ordinary differential equation model based on the law of mass action and the stochastic formulation, given by the chemical master equation, predict qualitatively different long term outcomes [6]. Such autocatalytic reactions occur, for example, in the misfolding of prion protein (PrP) in Creutzfeldt–Jakob disease [2] or the phosphorylation activation of certain enzymes [10]. Keizer's chemical reaction and several variations of it are also mentioned by Gardiner [3] and Van Kampen [11].

The reactions that form the basis for this observation, called Keizer's paradox, are

$$S + X \underset{k_{-1}}{\overset{k_1}{\rightleftharpoons}} 2X, \tag{1a}$$

$$X \xrightarrow{k_2} C, \tag{1b}$$

Reaction (1b) can be thought of as degradation. According to the law of mass action,

$$\frac{dx}{dt} = k_1 s x - k_{-1} x^2 - k_2 x, \tag{2}$$

where $x = [X]$, and $s = [S]$ are continuous state space variables. Assuming s is a constant, there are two steady states, an unstable solution with $x = 0$ and a stable positive solution (given $k_1 s > k_2$) $x = \frac{k_1 s - k_2}{k_{-1}}$. However, when this reaction is

modeled as a discrete stochastic birth-death process, the extinct state $x = 0$ is the unique absorbing state, and consequently the stochastic model predicts the species X will go extinct with probability 1.

Such contradictions between deterministic models and stochastic birth-death processes often appear partly because, in order to use a deterministic model, a large, but discrete, state space is treated as continuous. Indeed, almost any continuous population-tracking model can be thought of as an approximation to an underlying discrete stochastic process, as observed by Nåsell [9]. Such approximations are usually useful for some range of time or when the population in question is sufficiently large. However, if the population is small, a continuous state space cannot be easily justified, and, indeed, different behaviors are often observed. Similarly, in the long time limit, stochastic fluctuations can play an important role, even in large systems, and deterministic equilibria may be perturbed in significant ways. Indeed, for the above example, the typical behavior of the stochastic process is to rapidly approach a quasistationary distribution whose mean is close to the deterministic steady state, but then to go extinct on a much slower time scale because of random fluctuations. Consequently although extinction is sure probabilistically, the expected extinction time is quite large, becoming exponentially large as a function of system size, thus resolving the paradox.

Though at first glance it may seem so, our results do not conflict with the classic work done by Kurtz [7, 8] in comparing stochastic and deterministic models of chemical reactions. He proved that the ODE model is the infinite volume limit of the Markov process model. In this paper the volume in which the reactions occur is arbitrary but must remain finite for our results to hold.

The reaction (1) with S held constant was studied by Vellela and Qian [12]. They used numerical computations to estimate the expected extinction time as well as the time to reach the mean of the quasistationary distribution. Being numerical, their computations could only be performed for a truncated system, even though the state space is infinite. Vellela and Qian chose to truncate the state space at $N = 300$ because it was "sufficiently larger" than the deterministic steady state with their choice of parameter values.

In this paper we exploit the fact that in certain parameter ranges there is a separation of time scales, a fast time scale on which the stochastic process quickly approaches a quasistationary distribution very near the steady state concentration predicted by the deterministic model, and a slow time scale on which extinction occurs. With our analysis, using adiabatic elimination, or slow manifold dynamics, we calculate the time to extinction, showing that it grows exponentially with the size of the system.

Our analysis is applied to four variants of Keizer's paradox. First, we examine the reaction (1) with the substrate S held constant, and find analytical formulas for the mean extinction time. Second, we examine the reaction (1a) with the variation on the degradation reaction

$$X \xrightarrow{k_2} S, \tag{3}$$

and without the assumption that substrate S is held constant. This reaction scheme has the property that the total number of molecules, $n_S + n_X$, is constant, but exhibits the same paradoxical behavior as (1). Similar results for the mean extinction time are obtained as with the non-closed system.

Third, we consider the finite system obtained by the reactions in (1) without assuming the number of S molecules is held fixed. For this reaction, there is no conservation of total molecules, but instead the reaction occurs in a closed environment and is allowed to 'run down'. With this assumption, there is no paradox; both the stochastic model and the deterministic model predict extinction of the autocatalytic molecule X. However, the state of the system when X goes extinct is quantitatively different for the two models in terms of the number of S molecules which remain at extinction. Using our analysis, we are able to quantify these differences.

Fourth, we assume that the back-reaction rate in (1a) is proportional to S. With this modification S remains constant, so the analysis of this reaction is identical to that of the first case. However, when this autocatalytic reaction is coupled with the degradation reaction (3), the deterministic model has no positive steady state but predicts that S grows without bound, while the stochastic model once again predicts certain extinction. For this model, we calculate the extinction time for the stochastic process as well as the distribution for the substrate species S when X goes extinct.

Finally, by bounding the spectral gaps of the necessary matrices and operators, we provide rigorous estimates for parameter ranges within which the time scale separation is sufficient to permit a quasistationary - slow manifold analysis.

2. **Keizer's paradox.**

2.1. **Problem formulation.** First, we consider the original problem proposed by Keizer [6]. In this problem, S is held fixed at, say, n_S molecules. (The mechanism by which this is accomplished is not stated, although this is necessarily an open system.) Consequently, since n_S does not change, the only species we need to track is X.

As noted in the introduction, modeling this reaction using ordinary differential equations and the law of mass action predicts that the concentration of X tends to a positive steady state.

For the stochastic description of this process, the state of the system is determined by the number n of X molecules, $n = 0, 1, 2, \cdots$. A state transition diagram is shown in Figure 1. The transition rate parameters $\hat{k}_1$, $\hat{k}_{-1}$, and $\hat{k}_2$ are related to the chemical reaction rates in (1) by

$$\hat{k}_1 = \frac{k_1}{V}, \tag{4a}$$

$$\hat{k}_{-1} = \frac{k_{-1}}{V}, \tag{4b}$$

$$\hat{k}_2 = k_2, \tag{4c}$$

where V is the volume of the system.
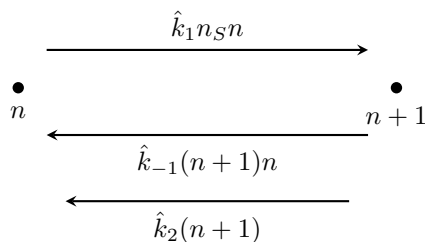
FIGURE 1. State diagram for the stochastic system with a semi-infinite state space.

The chemical master equations for this process are the infinite system of ordinary differential equations

$$
\begin{cases}
\dfrac{dp_0}{dt} = \hat{k}_2 p_1, \\[2mm]
\dfrac{dp_1}{dt} = (2\hat{k}_{-1} + 2\hat{k}_2)p_2 - (\hat{k}_2 + \hat{k}_1 n_S)p_1, \\[2mm]
\quad\vdots \\[2mm]
\dfrac{dp_n}{dt} = \hat{k}_1 n_S(n-1)p_{n-1} + (\hat{k}_{-1}(n+1)n + \hat{k}_2(n+1))p_{n+1} \\[2mm]
\qquad\quad - (\hat{k}_{-1}n(n-1) + \hat{k}_1 n_S n + \hat{k}_2 n)p_n, \\[2mm]
\quad\vdots
\end{cases}
\tag{5}
$$

where $p_n(t)$ is the probability that the system is in state n, *i.e.* has n molecules of species X, at time t. We nondimensionalize this system with the rescaling of time $\hat{t} = \hat{k}_1 n_S t$. We can now write this system as the "matrix" equation

$$
\frac{dp}{d\hat{t}} = (A + \varepsilon B)p,
\tag{6}
$$

where $\varepsilon = \hat{k}_2/(\hat{k}_1 n_S)$. The word matrix above is in quotes because A and B are not matrices in the usual sense, but rather are linear operators on ℓ^1, and $p = \begin{bmatrix} p_0, & p_1, & p_2, & \dots \end{bmatrix}^{\mathrm{T}} \in \ell^1$ is a probability distribution over the natural numbers. That said, A is the tridiagonal operator

$$
A = \begin{bmatrix}
0 & 0 & 0 & \dots & & & \dots \\
0 & -1 & 2\gamma^{-1} & & & & \\
0 & 1 & -2-2\gamma^{-1} & 6\gamma^{-1} & & & \\
\vdots & & \ddots & \ddots & \ddots & & \\
& & & (n-1) & -n-n(n-1)\gamma^{-1} & n(n+1)\gamma^{-1} & \\
\vdots & & & & \ddots & \ddots & \ddots
\end{bmatrix}
\tag{7}
$$

with $\gamma = \hat{k}_1 n_S / \hat{k}_{-1}$, and

$$
B = \begin{bmatrix}
0 & 1 & 0 & \dots & & & \dots \\
0 & -1 & 2 & & & & \\
0 & 0 & -2 & 3 & & & \\
\vdots & & & \ddots & \ddots & & \\
& & & & -n & (n+1) & \\
\vdots & & & & & \ddots & \ddots
\end{bmatrix}
\tag{8}
$$

is upper triangular. Because our state space includes the state $n = 0$, indices for all elements of and operators on ℓ^1 herein begin at 0.

2.2. **Slow manifold reduction.** The purpose of writing these two operators separately is to motivate a slow manifold reduction treating ε as a small parameter. This has been called adiabatic elimination of fast variables [3]. In fact, if the amount of substrate, S, is sufficiently large, then ε is small, and the nullspace of A is a slow manifold. Our first step, then, is to find the null vectors for the matrix A. One can easily see that $\phi = \begin{bmatrix} 1, & 0, & 0, & \dots \end{bmatrix}^{\mathrm{T}}$ is a null vector since the first column of A is all zeros. However, A has another null vector, which we call π. Forcing the distribution π to be mutually exclusive to ϕ gives $\pi_0 = 0$. In other words, the distribution π corresponds to having zero probability of being in the extinct state. The remaining entries are found using a simple inductive argument (see Van Kampen [11]) to be

$$
\pi_n = \frac{1}{n!} \gamma^{n-1} \pi_1, \qquad n = 2, 3, \dots
\tag{9}
$$

with the condition $\sum_j \pi_j = 1$. So,

$$
\pi_n = \frac{\gamma^n}{n!} \left(e^\gamma - 1 \right)^{-1}, \qquad n = 1, 2, \dots.
\tag{10}
$$

This is a zero-truncated Poisson distribution with parameter γ. It has mean

$$
\mu = \gamma \frac{e^\gamma}{e^\gamma - 1} \approx \gamma = \frac{\hat{k}_1 n_S}{\hat{k}_{-1}},
\tag{11}
$$

which, in units of concentration, is $\frac{k_1 s}{k_{-1}}$, and is greater than the deterministic steady state $\frac{k_1 s - k_2}{k_{-1}}$, but agrees exactly with the deterministic steady state if we were only to consider reaction (1a).

We examine the non-zero eigenvalues of the matrix A in section 4. In fact, the reduction of this system to the nullspace of A must be justified by a more rigorous separation of time scales. This requires a better understanding of the spectra of A and B. We show, in section 4, that the remaining eigenvalues of A are greater than $1/3$ in magnitude. So, other modes are damped out exponentially. This means that, given some initial condition $p(0)$, there is an initial layer before the solution settles onto the two-dimensional slow manifold spanned by ϕ and π. So, after a short, $O(1)$, initial time, the solution to (6) will be of the form

$$
p(\hat{t}) = c_0 \phi + c_1 \pi + O(\varepsilon),
\tag{12}
$$

where $c_{0,1}$ are slowly varying scalar-valued functions of $\hat{t}$ and the $O(\varepsilon)$ contribution is not in the range of ϕ and π. Here, $c_0 = p_0(\hat{t})$. Projecting onto the nullspace of A

by multiplying both sides of (6) on the left by $\mathbf{1}^{\mathrm{T}}$, the row-vector with a 1 in every component, gives, to leading order in ε,

$$\frac{dc_0}{d\hat{t}} + \frac{dc_1}{d\hat{t}} = 0. \tag{13}$$

Thus, $c_0 + c_1$ is conserved, and in fact, since $\sum p_j = 1$,

$$c_1 = 1 - c_0. \tag{14}$$

The projection of (6) given by multiplying both sides on the left by ϕ^{T} is

$$\frac{dc_0}{d\hat{t}} = c_1 \varepsilon \sum_{j=0}^{\infty} B_{0,j} \pi_j$$
$$= \varepsilon \gamma \left(e^\gamma - 1\right)^{-1} c_1. \tag{15}$$

Substituting (14) into (15) and solving the resulting equation gives

$$c_0(\hat{t}) = 1 - (1 - c_0(\hat{t}^*)) \exp\left(-\frac{\varepsilon\gamma}{e^\gamma - 1}\hat{t}\right). \tag{16}$$

Hence, $p_0 \to 1$ exponentially in time once the solution is on this slow manifold. However, the rate at which this occurs is extremely slow, because the denominator in the exponent of (16) is exponentially large. The use of $\hat{t}^*$ indicates the short time it takes to get to this manifold, and $c_0(\hat{t}^*)$ is the location on manifold the initial conditions determine the solution will approach in that short time. This means that the species X goes extinct with probability 1. The relevant question, though, is how long it takes before this occurs.

If we make the further approximation that $c_0(\hat{t}^*) = 0$, that is, that the system starts out in quasistationary state, we can find that the expected nondimensional time to extinction $\hat{\tau}$ is given by

$$\hat{\tau} = \int_0^\infty \hat{t} c_0'(\hat{t}) \, d\hat{t}. \tag{17}$$

Expressed in dimensional time, the time to extinction is

$$\tau = \frac{\hat{k}_{-1}}{\hat{k}_2 \hat{k}_1 n_S} \left(\exp\left(\frac{\hat{k}_1 n_S}{\hat{k}_{-1}}\right) - 1 \right). \tag{18}$$

This compares favorably to the numerical study done by Vellela and Qian[12], and provides an analytical estimate for the extinction time. Using the same parameters they used, namely $k_1 = k_{-1} = k_2 = .55$, and $n_S = 100$ we find

$$\tau \approx 4.89 \times 10^{41}. \tag{19}$$

Having made the reduction in (12) it is difficult to get a handle on τ_1, the expected time to extinction given the initial condition $p_n(0) = \delta_{1,n}$. However, using these same parameters, we can calculate $\tau_{\mu,1}$, the expected time to reach μ, the mean of the distribution π. First, we calculate the splitting probability $\theta_{\mu,1}$. This is the probability that, starting at state 1, the reaction reaches state μ (or nearest integer) before reaching state 0. Van Kampen calculates this for a general birth-death process on pp. 298-300 [11]. For our parameter values, $\mu = 100$ and

$$\theta_{\mu,1} \approx 0.9899. \tag{20}$$

This means that, with very high probability, the process will reach the mean of the quasistationary distribution before going extinct, another hint at justification for

our reduction to the aforementioned manifold. We use this, and the other splitting probabilities, to compute

$$\tau_{\mu,1} = \frac{\sum_{m=1}^{\mu-1} \sum_{k=1}^{m} \frac{\theta_{\mu,k}}{g_k} \prod_{j=k+1}^{m} \frac{r_j}{g_j}}{\theta_{\mu,1} \sum_{m=0}^{\mu-1} \prod_{i=1}^{m} \frac{r_i}{g_i}}, \tag{21}$$

where empty products are equal to 1, and

$$g_j = \hat{k}_1 n_S j, \tag{22a}$$

$$r_j = \hat{k}_{-1} j(j-1) + \hat{k}_2 j \tag{22b}$$

are the birth and death rates, respectively. With the parameter values above, numerically we obtain

$$\tau_{\mu,1} \approx .1492. \tag{23}$$

Hence, not only does the process tend toward the mean of π, it does so many orders of magnitude more quickly than the expected waiting time for an extinction event.

3. **Variations on the original reaction.**

3.1. **Closed and conserved.** We now turn our attention to the variation on the reaction scheme given by reactions (1a) and (3). We suppose that the reactions occur in a closed environment. It is clear, then, that $N = n_X + n_S$ is a conserved quantity, so n_S is no longer a constant. The total concentration $s^* = x + s$ is similarly conserved. Then, the deterministic ODE model for these reactions is

$$\frac{dx}{dt} = k_1 x(s^* - x) - k_{-1} x^2 - k_2 x, \tag{24}$$

which has the unique positive stable steady state (provided $k_1 s^* > k_2$)

$$x^* = \frac{k_1 s^* - k_2}{k_1 + k_{-1}}. \tag{25}$$

However, consideration of the chemical master equation gives the same paradox as with the infinite-dimensional system. Letting $\tilde{p}$ denote the probability density vector, we write

$$\frac{d\tilde{p}}{d\tilde{t}} = (\tilde{A} + \tilde{\varepsilon}\tilde{B})\tilde{p}, \tag{26}$$

where

$$\tilde{A} = \frac{1}{N} \begin{bmatrix} 0 & 0 & & & & \\ 0 & -(N-1) & 2\tilde{\gamma}^{-1} & & & \\ & (N-1) & -2(N-2)-2\tilde{\gamma}^{-1} & 6\tilde{\gamma}^{-1} & & \\ & & \ddots & \ddots & \ddots & \\ & & & & & -N(N-1)\tilde{\gamma}^{-1} \\ & & & & (N-1) & N(N-1)\tilde{\gamma}^{-1} \end{bmatrix}, \tag{27}$$

and

$$\tilde{B} = \begin{bmatrix} 0 & 1 & & & & \\ 0 & -1 & 2 & & & \\ & & -2 & 3 & & \\ & & & \ddots & \ddots & \\ & & & & -(N-1) & N \\ & & & & & -N \end{bmatrix}, \tag{28}$$

with $\tilde{\gamma} = \hat{k}_1/\hat{k}_{-1}$ and $\tilde{\varepsilon} = \hat{k}_2/(\hat{k}_1 N)$. Here, we have nondimensionalized time in (26) by the scaling $\tilde{t} = \hat{k}_1 N t$.

Once again, the only stationary probability distribution for (26) is the vector ψ which is simply ϕ truncated to be length $N + 1$. Indeed, the species X goes extinct almost surely. However, we can apply the same technique here to determine the time scale on which extinction occurs. We perform a slow manifold reduction treating $\tilde{\varepsilon}$ as a small parameter. As above, we leave the formal comparison of the spectra of $\tilde{A}$ and $\tilde{\varepsilon}\tilde{B}$ to section 4. Besides ψ, the only other probability vector in the nullspace of $\tilde{A}$ is ρ, given by

$$\rho_n = \tilde{\gamma}^n \binom{N}{n} \left((1 + \tilde{\gamma})^N - 1 \right)^{-1} \qquad n = 1, 2, \ldots, N, \tag{29}$$

with $\rho_0 = 0$. Interestingly, if we make the assumption that $\hat{k}_1$ is inversely proportional to N and take the limit as $N \to \infty$, then ρ limits to a zero-truncated Poisson distribution similar, but not identical to (10). However, there is no physically natural limit in which the systems compare directly. The distribution in (29) has mean

$$\tilde{\mu} = N\tilde{\gamma} \frac{(1 + \tilde{\gamma})^{N-1}}{(1 + \tilde{\gamma})^N - 1}. \tag{30}$$

As before, we assume that after an initial layer, solutions of (26) take the form

$$\tilde{p}(\tilde{t}) = d_0 \psi + d_1 \rho + O(\tilde{\varepsilon}). \tag{31}$$

This is justified in section 4. Then, applying the same technique, multiplying (26) on the left by $\mathbf{1}^{\mathrm{T}}$ and then, separately by ψ^{T}, we arrive at

$$d_0(\tilde{t}) = 1 - (1 - d_0(\tilde{t}^*)) \exp\left(-\frac{\varepsilon \gamma N}{(1 + \tilde{\gamma})^N - 1} \tilde{t} \right). \tag{32}$$

Since $d_0(t)$ is the probability that the species X has gone extinct by time t, we see that, if $d_0(\tilde{t}^*) = 0$, the expected extinction time (in original units of time) for this finite-dimensional problem is

$$\tilde{\tau} = \frac{\hat{k}_{-1}}{\hat{k}_2 \hat{k}_1} \frac{\left(1 + \frac{\hat{k}_1}{\hat{k}_{-1}} \right)^N - 1}{N}. \tag{33}$$

Choosing the same rates as above, $k_1 = k_{-1} = k_2 = .55$, and letting $N = 100$, we find

$$\tilde{\tau} \approx 2.305 \times 10^{28}. \tag{34}$$

For comparison, since this system is finite, we can compute $\tilde{\tau}_1$, the expected time to extinction from state 1, exactly. Using a theorem stated by Allen [1] pp. 240–241, we find

$$\tilde{\tau}_1 \approx 4.6572 \times 10^{26}. \tag{35}$$

It should not be a surprise that this is smaller than our estimate from the slow manifold reduction, since the initial condition is far closer to extinction. Also for comparison, with these parameter values, $\tilde{\mu} \approx 50$, the probability of reaching the integer state nearest $\tilde{\mu}$ given the initial condition of state 1 is

$$\tilde{\theta}_{\tilde{\mu},1} \approx 0.9898, \tag{36}$$

and the expected time to arrive at that state is

$$\tilde{\tau}_{\tilde{\mu},1} \approx .1355. \tag{37}$$

Again, we see the near certainty of arriving at $\tilde{\mu}$ before extinction and the expectation of doing so many orders of magnitude faster than an extinction event can occur.

3.2. **Closed with degradation.** Now we consider both reactions in (1) occurring in a closed environment. The initial number of molecules in the system is $N = n_S + n_X$, but when an S molecule is converted, it does not get replaced, and when an X molecule degrades it is gone for good. We now must track two variables, the concentrations of S and X. The deterministic system is

$$\frac{dx}{dt} = k_1 sx - k_{-1} x^2 - k_2 x,$$
$$\frac{ds}{dt} = -k_1 sx + k_{-1} x^2. \tag{38}$$

With these conditions, the deterministic and stochastic models agree in that they both predict extinction for the autocatalytic molecule X. This is easy to see with the deterministic system since

$$\frac{d}{dt}(x + s) = -k_2 x \leq 0, \tag{39}$$

and it is certainly not surprising with the stochastic system. The interesting question here is how many molecules of S remain when X does go extinct.

The deterministic model for this system has, as nullclines, two parallel lines with slope k_{-1}/k_1: one which passes through the origin and one which passes through the s axis at $s = k_2/k_1$. The entire s axis is the only set of fixed points. This corresponds to the termination of the reaction if species X goes extinct. There is also an invariant manifold between the two parallel nullclines. It is

$$\left\{ (x, s) \geq 0 \mid s = \frac{k_{-1}}{k_1} \left(x + \frac{k_2}{k_1 + k_{-1}} \right) \right\}. \tag{40}$$

To get a clearer sense of how this system behaves, we make the 2×2 change of variables

$$m = x + s,$$
$$u = k_1 s - k_{-1} \left(x + \frac{k_2}{k_1 + k_{-1}} \right), \tag{41}$$

which gives us equations for $\dot{m}$ and $\dot{u}$. Conveniently, we can solve for u as a function of m by taking the ratio

$$\frac{\dot{u}}{\dot{m}} = \frac{du}{dm} = \frac{k_1 + k_{-1}}{k_2} u. \tag{42}$$

Then

$$u = u_0 \, e^{\frac{k_1 + k_{-1}}{k_2}(m - m_0)}. \tag{43}$$

From (39) we know that m approaches 0 from above in forward time, so (43) implies that u approaches the exponentially small quantity $u_0 \, e^{\frac{k_1 + k_{-1}}{k_2}(-m_0)}$. The axis given by $u = 0$ corresponds with the manifold specified in (40). Hence, we see that from any initial condition trajectories move exponentially close to this manifold before the species X can go extinct. Therefore, the deterministic system predicts that when there are no more molecules of X left to drive the reaction, there will remain in solution a concentration of S which is approximately

$$s^\infty = \frac{k_{-1} k_2}{k_1 (k_1 + k_{-1})}. \tag{44}$$

The stochastic model for the process is represented by the diagram in Figure 2. Along each diagonal in the figure the transition rates are the same as in the matrix $\tilde{A}$.
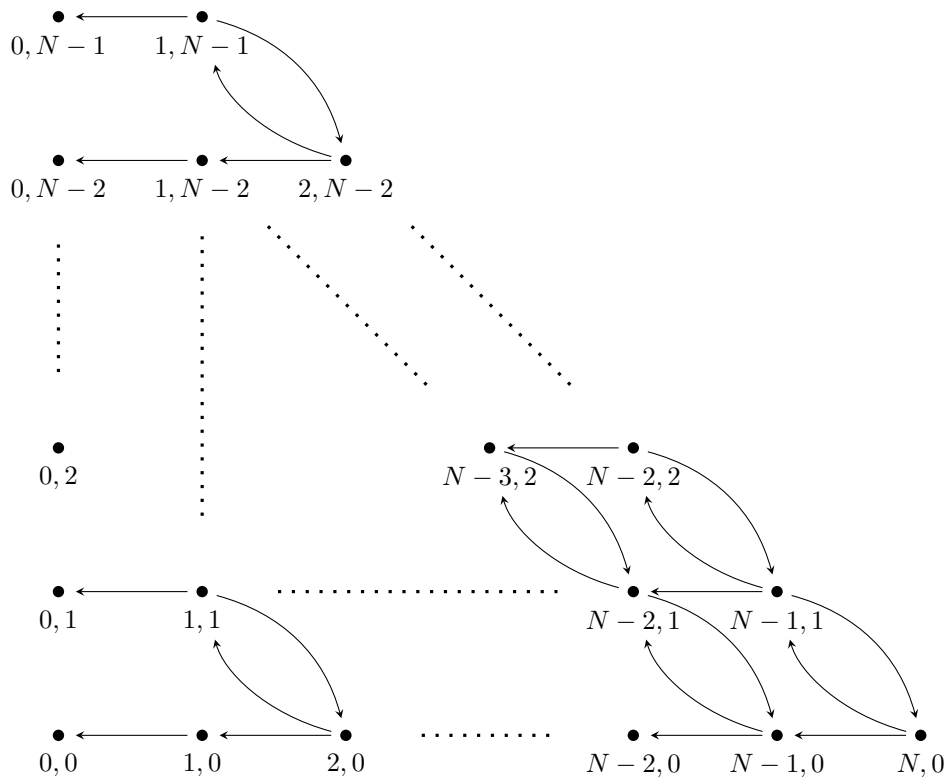

FIGURE 2. State diagram for the stochastic system with finite state space. Coordinates in the diagram are (n_X, n_S).

The horizontal arrows from each state to the state on its left represent degradation of X. It is clear that each state $(0, n)$ for $n = 0, 1, \ldots, N-1$ is absorbing. In order to understand how the state probabilities for this system evolve, we notice that if we add the equations corresponding to a given diagonal we get

$$
\begin{cases}
\dfrac{dP_N}{dt} = \displaystyle\sum_{j=1}^{N} -\hat{k}_2 j p_{j, N-j}, \\[2mm]
\quad \vdots \\[2mm]
\dfrac{dP_Q}{dt} = \displaystyle\sum_{j=1}^{Q+1} \hat{k}_2 j p_{j, (Q+1)-j} - \sum_{j=1}^{Q} \hat{k}_2 j p_{j, Q-j}, \\[2mm]
\quad \vdots \\[2mm]
\dfrac{dP_0}{dt} = \hat{k}_2 p_{1,0},
\end{cases}
\tag{45}
$$

where

$$P_Q = \sum_{j=0}^{Q} p_{j,Q-j} \tag{46}$$

is the probability of being in any state on the diagonal $n_S + n_X = Q$.

We now use the quasistationary approximation from (29) conditioned on the event that the system is in some state on diagonal Q. The validity of this approximation is discussed below. So then, applying Bayes' Theorem and reordering the equations, the system decouples to the $2N$-dimensional system

$$
\begin{cases}
\dfrac{dP_{1'}}{dt} = (\omega_2 - \alpha_2)P_{2'} - \omega_1 P_{1'}, \\[2mm]
\quad\vdots \\[2mm]
\dfrac{dP_{Q'}}{dt} = (\omega_{Q+1} - \alpha_{Q+1})P_{(Q+1)'} - \omega_Q P_{Q'}, \\[2mm]
\quad\vdots \\[2mm]
\dfrac{dP_{N'}}{dt} = -\omega_N P_{N'},
\end{cases}
\tag{47a}
$$

$$
\begin{cases}
\dfrac{dp_{0,0}}{dt} = \alpha_1 P_{1'}, \\[2mm]
\quad\vdots \\[2mm]
\dfrac{dp_{0,Q}}{dt} = \alpha_{Q+1} P_{(Q+1)'}, \\[2mm]
\quad\vdots \\[2mm]
\dfrac{dp_{0,N-1}}{dt} = \alpha_N P_{N'},
\end{cases}
\tag{47b}
$$

where

$$P_{Q'} = P_Q - p_{0,Q} \tag{48}$$

is the probability of being on diagonal Q but not in state $(0, Q)$, denoted by the prime. The binomial theorem gives us expressions for the α_Q's and ω_Q's:

$$\alpha_Q = \frac{\hat{k}_2 \hat{k}_1}{\hat{k}_{-1}} Q \left(\left(1 + \frac{\hat{k}_1}{\hat{k}_{-1}}\right)^Q - 1 \right)^{-1}, \tag{49a}$$

$$\omega_Q = \alpha_Q \left(1 + \frac{\hat{k}_1}{\hat{k}_{-1}}\right)^{Q-1}. \tag{49b}$$

If we let $P = \begin{bmatrix} P_{1'}, & \ldots, & P_{N'} \end{bmatrix}^{\mathrm{T}}$, and $q = \begin{bmatrix} p_{0,0}, & \ldots, & p_{0,N-1} \end{bmatrix}^{\mathrm{T}}$, then we can rewrite (47) as

$$\dot{P} = \Omega P, \tag{50a}$$
$$\dot{q} = \Lambda P. \tag{50b}$$

The matrix Λ is simply the diagonal matrix of α_Q's, and Ω is upper triangular with diagonal entries $-\omega_1, \ldots, -\omega_N$, hence, it is invertible and has negative eigenvalues. This is crucial, because solving (50) yields

$$q(t) = \Lambda \Omega^{-1} \left(e^{t\Omega} - I\right) P(0). \tag{51}$$

Then, we define

$$q^\infty = \lim_{t \to \infty} q(t) = -\Lambda \Omega^{-1} P(0). \tag{52}$$

This is the approximate distribution of how many S molecules remain once the species X goes extinct. If we assume that the reaction begins with N molecules, then the initial condition is $P(0) = \begin{bmatrix} 0, & 0, & \dots, & 1 \end{bmatrix}^{\mathrm{T}}$, and the terminal probability distribution for the species S simplifies drastically to

$$q_n^\infty = \left(1 + \frac{\hat{k}_1}{\hat{k}_{-1}}\right)^{-n} \prod_{j=n+2}^{N} \left(1 - \left(1 + \frac{\hat{k}_1}{\hat{k}_{-1}}\right)^{1-j}\right), \qquad n = 0, 1, \dots, N-1, \tag{53}$$

where, again, empty products are unity. Note that this distribution is independent of k_2, due to the reduction.

The use of this approximation is not well justified on every diagonal because it relies on having a large enough system. When Q is small, the system is not always likely to reach a quasistationary distribution. However, we see, upon inspecting the distribution (53), the range of Q for which the quasistationary reduction might be considered accurate. On each diagonal which affects the exit distribution significantly, we need $\tilde{\varepsilon}$ relatively small in order to have a separation of time scales. Decreasing $\hat{k}_2$ or increasing $\hat{k}_1$ achieves this effect. In a word, we need $\hat{k}_2/(\hat{k}_1 Q) \ll 1/3$ for all Q in the bulk of the distribution (53).

In Figure 3, we compare this predicted distribution to the results of several thousand Gillespie simulations for a range of parameter values. Without loss of generality, we can fix $\hat{k}_1 = 1$ for all simulations, because only ratios of parameters affect the results. The results of simulations shown in Figures 3(a), 3(c), and 3(e) agree closely with the predicted distribution. Figures 3(b), 3(d), and 3(f) show results where $\hat{k}_2$ is increased enough to cause discrepancy between the simulated and predicted distributions. The only case in which the deterministic model prediction is close to the mean of any of these distributions is if $\hat{k}_{-1}$ is small. In Figure 4, we show how the means of these distributions depend on combinations of parameters. As stated, there is good agreement between the predicted mean and the simulated mean when $\hat{k}_2$ is sufficiently small or when $\hat{k}_{-1}$, and, hence, any relevant values of Q, are sufficiently large. Increasing $\hat{k}_2$ invalidates the quasistationary assumption. We also see in both figures, 3 and 4, that the deterministic model fails to capture the behavior of this distribution.

3.3. Trimolecular reaction.
The final variation on our reaction scheme is the autocatalytic reaction

$$S + X \underset{k'_{-1}}{\overset{k_1}{\rightleftharpoons}} S + 2X, \tag{54}$$

which can also be written as

$$S + X \underset{k'_{-1}S}{\overset{k_1}{\rightleftharpoons}} 2X, \tag{55}$$

When this reaction is coupled with the degradation reaction (1b), the master equations are identical to those for (1) with S held constant provided k_{-1} is replaced by $k'_{-1}S$, or equivalently $\hat{k}_{-1}$ is replaced by $\hat{k}'_{-1} n_S$, where $\hat{k}'_{-1} = \frac{k'_{-1}}{V^2}$.

(a) $\hat{k}_{-1} = 2$, $\hat{k}_2 = 1$

(b) $\hat{k}_{-1} = 2$, $\hat{k}_2 = 10$

(c) $\hat{k}_{-1} = 30$, $\hat{k}_2 = 1$

(d) $\hat{k}_{-1} = 30$, $\hat{k}_2 = 10$

(e) $\hat{k}_{-1} = 70$, $\hat{k}_2 = 1$
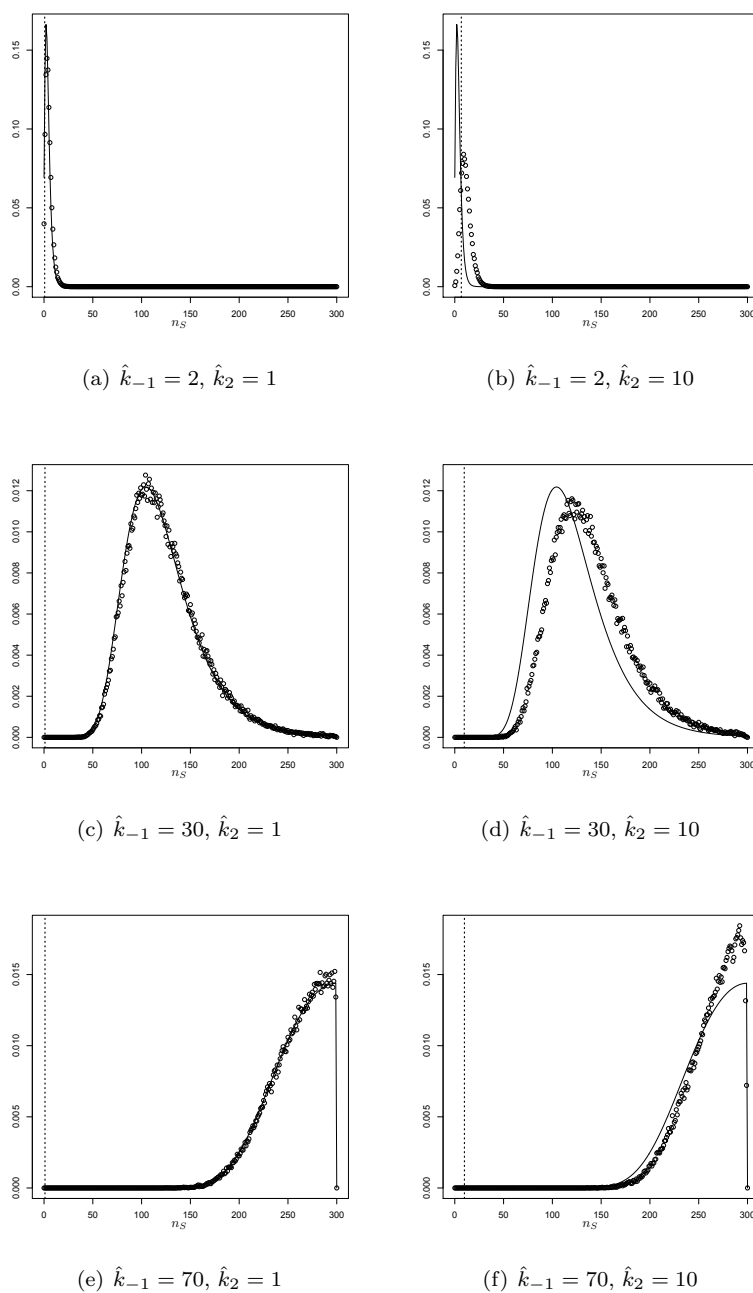
(f) $\hat{k}_{-1} = 70$, $\hat{k}_2 = 10$

FIGURE 3. Comparisons of Gillespie simulations with predicted distributions. Each circle represents the fraction out of 100,000 trials for which n_S molecules remained at extinction. Each vertical dotted line is at the value $V s^\infty$ from (44). For each figure, $\hat{k}_1 = 1$.
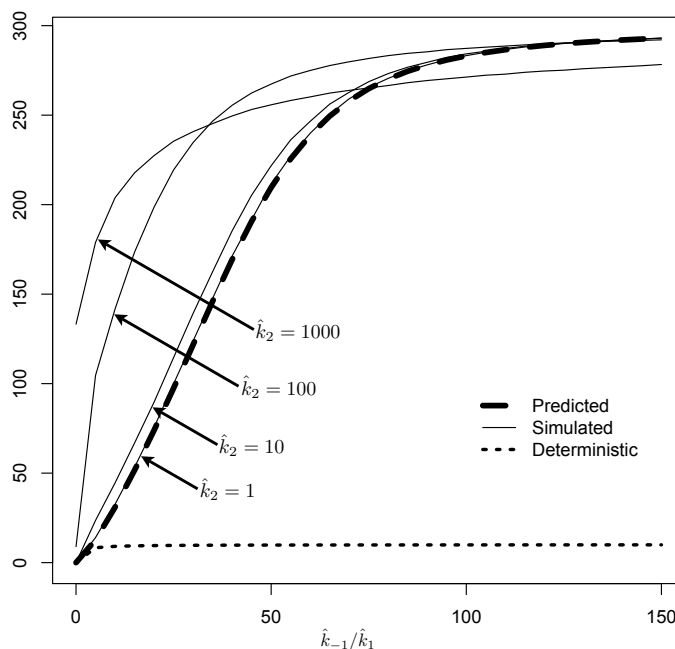
FIGURE 4. The fine dotted line is Vs^∞ from (44) with $\hat{k}_2 = 10$. The thick dashed line is $\langle q^\infty \rangle$ from (53), which is independent of $\hat{k}_2$. Solid lines are the average remaining S molecules from Gillespie simulations for a range of $\hat{k}_2$. Initial conditions for these simulations are chosen uniformly on $n_S + n_X = 300$. Since we are only concerned with ratios of parameters, $\hat{k}_1 = 1$ for each curve.

We observe a more interesting phenomenon when reaction (54) is coupled with the degradation reaction (3). With these two reactions, the deterministic model is

$$\begin{aligned}
\frac{dx}{dt} &= k_1 sx - k'_{-1} sx^2 - k_2 x, \\
\frac{ds}{dt} &= k_2 x.
\end{aligned} \tag{56}$$

With sufficiently large initial conditions (for example, $s > \frac{k_2}{k_1}$, $x > 0$), the solution to these equations predicts that [S] grows without bound, while [X] tends to $\frac{k_1}{k'_{-1}}$.

The chemical master equation is doubly infinite, and, again, predicts certain extinction for X. We ask the same question here as in the previous section: given an initial number of molecules in solution, how many S molecules remain when X is depleted?

The Kolmogorov equations needed to answer this question tell us how $P_{S=n}$, the probability that S is in state n, evolves. We write them as

$$\begin{cases} \dfrac{dP_{S=0}}{dt} = -\hat{k}_2 \sum_{j=1}^{\infty} j P_{X=j|S=0} P_{S=0}, \\[2ex] \dfrac{dP_{S=n}}{dt} = \hat{k}_2 \sum_{j=1}^{\infty} j P_{X=j|S=n-1} P_{S=n-1} - \hat{k}_2 \sum_{j=1}^{\infty} j P_{X=j|S=n} P_{S=n}, \qquad n = 1, 2, \ldots \end{cases}$$

(57)

Bayes' Theorem allows us to rewrite these as

$$\begin{cases} \dfrac{dP_{S=0}}{dt} = -\hat{k}_2 \sum_{j=1}^{\infty} j P_{X=j|X\neq0,S=0} P_{X\neq0|S=0} P_{S=0}, \\[2ex] \dfrac{dP_{S=n}}{dt} = \hat{k}_2 \sum_{j=1}^{\infty} j \left(P_{X=j|X\neq0,S=n-1} P_{X\neq0|S=n-1} P_{S=n-1} \right. \\[2ex] \qquad\qquad\qquad \left. -P_{X=j|X\neq0,S=n} P_{X\neq0|S=n} P_{S=n} \right). \end{cases}$$

(58)

Using the same argument we make in the previous section, we make the quasistationary reduction

$$P_{X\neq0|S=n} = 1 - c_0$$

(59)

from (16) and

$$P_{X=j|X\neq0,S=n} = \pi_j$$

(60)

from (10), each of which have γ replaced by $\gamma' = \frac{\hat{k}_1}{\hat{k}'_{-1}}$. Hence, π_j is independent of n_s, and

$$\sum_{j=1}^{\infty} j P_{X=j|X\neq0} = \mu' = \gamma' \frac{e^{\gamma'}}{e^{\gamma'} - 1},$$

(61)

as in (11). Then (58) simplifies to

$$\begin{cases} \dfrac{dP_{S=0}}{dt} = -\dfrac{\hat{k}_2 \gamma' e^{\gamma'}}{e^{\gamma'} - 1} \exp\left(\dfrac{-\hat{k}_2 \gamma' t}{e^{\gamma'} - 1} \right) P_{S=0}, \\[3ex] \dfrac{dP_{S=n}}{dt} = \dfrac{\hat{k}_2 \gamma' e^{\gamma'}}{e^{\gamma'} - 1} \exp\left(\dfrac{-\hat{k}_2 \gamma' t}{e^{\gamma'} - 1} \right) \left(P_{S=n-1} - P_{S=n} \right). \end{cases}$$

(62)

We simplify even further by letting

$$\frac{df}{dt} = \frac{\hat{k}_2 \gamma' e^{\gamma'}}{e^{\gamma'} - 1} \exp\left(\frac{-\hat{k}_2 \gamma' t}{e^{\gamma'} - 1} \right).$$

(63)

Then

$$\begin{cases} \dfrac{dP_{S=0}}{df} = -P_{S=0}, \\[2ex] \dfrac{dP_{S=n}}{df} = P_{S=n-1} - P_{S=n}. \end{cases}$$

(64)

This is now a standard description of a Poisson process with parameter 1. Solutions of (64) are

$$P_{S=n}(f) = \begin{cases} 0 & n < m, \\[1ex] \dfrac{f^{n-m} e^{-f}}{(n-m)!} & n \geq m, \end{cases}$$

(65)

where

$$f = \int_0^t \frac{\hat{k}_2 \gamma' e^{\gamma'}}{e^{\gamma'} - 1} \exp\left(\frac{-\hat{k}_2 \gamma' s}{e^{\gamma'} - 1}\right) ds = e^{\gamma'} \left(\exp\left(\frac{-\hat{k}_2 \gamma' t}{e^{\gamma'} - 1}\right) - 1\right), \qquad (66)$$

and m is the initial number of S molecules. So then, letting $t \to \infty$, we find the predicted probability density for the number of S molecules remaining when all X is depleted. It is the shifted Poisson distribution

$$P_{S=n}^\infty = \begin{cases} 0 & n < m \\ \frac{e^{\gamma'(n-m)} e^{\left(-e^{\gamma'}\right)}}{(n-m)!} & n \geq m, \end{cases} \qquad (67)$$

which has mean $e^{\gamma'} + m$. It is nigh impossible to compare this distribution with the results of simulations because the time to extinction of X is so long for this process.

4. **Spectral gap analysis.** Our final objective is to justify the claims made in the previous sections. That is, we want to show that an initial distribution will move sufficiently quickly onto the slow manifold to consider the slow manifold reductions valid. This is done by examining the spectrum of the operator A. In particular, we wish to show that the non-zero eigenvalue with least magnitude is bounded some sufficient distance from the origin to consider ε and $\tilde{\varepsilon}$ comparatively small parameters. First, we consider the spectrum of the matrix $\tilde{A}$.

To this end we take advantage of the work by Granovsky and Zeifman [4, 5] in bounding the spectral gap β of birth-death processes, which is the minimum of all moduli of the non-zero eigenvalues of the matrix. In particular, they defined $\mathscr{C}$ to be the set of all real matrices $C = \{c_{ij}, i, j = 1, \ldots, N\}$ with non-negative off-diagonal entries,

$$c_{ij} \geq 0, \quad i \neq j, \quad i, j = 1, \ldots, N \qquad (68)$$

and non-positive column sums

$$c_j = \sum_{i=1}^N c_{ij} \leq 0, \quad j = 1, \ldots, N. \qquad (69)$$

Then, they proved that for any matrix $C \in \mathscr{C}$, the magnitude of the smallest eigenvalue

$$|z_0| = \min\{|z_i|, z_i \in \sigma(C)\} \qquad (70)$$

satisfies

$$-\bar{c} \leq |z_0| \leq -\underline{c} \qquad (71)$$

where

$$\begin{aligned} \underline{c} &= \min\{c_j, \ j = 1, \ldots, N\} \\ \bar{c} &= \max\{c_j, \ j = 1, \ldots, N\}. \end{aligned} \qquad (72)$$

4.1. **Spectral gap in the finite case.** The matrix $\tilde{A}$ in (26) is a $\mathbb{W}$-matrix as defined by Van Kampen [11], so every column sum is 0. Hence, the bounds given in (71) are not immediately useful for bounding the spectral gap of $\tilde{A}$. However, the entire first column and first row of $\tilde{A}$ are zeros. Considering the matrix $\bar{A}$ obtained by deleting this row and column, $\bar{A}$ is an irreducible $\mathbb{W}$-matrix and it has the null vector $\begin{bmatrix} \rho_1, & \ldots, & \rho_N \end{bmatrix}^{\mathrm{T}}$. We only consider matrices and operators truncated thus for the remainder of this text.

Granovsky and Zeifman noticed that the differential equation

$$\frac{dp}{dt} = \bar{A}p \tag{73}$$

can be transformed via

$$p_1(t) = 1 - \sum_{i=2}^{N} p_i(t) \tag{74}$$

into the equivalent equation

$$\frac{dy}{dt} = \bar{B}y(t) + f, \tag{75}$$

where

$$\bar{B} = \{\bar{a}_{ij} - \bar{a}_{i1}, \ \ i,j = 2,\ldots,N\},$$
$$y(t) = \begin{bmatrix} p_2(t), & \ldots, & p_N(t) \end{bmatrix}^{\mathrm{T}} \tag{76}$$
$$f = \begin{bmatrix} \bar{a}_{21} & \ldots, & \bar{a}_{N1} \end{bmatrix}^{\mathrm{T}}.$$

This is useful for determining β because $\sigma(\bar{B}) = \sigma(\bar{A})/\{0\}$. Hence, the smallest eigenvalue in $\sigma(\bar{B})$ is the spectral gap for our original matrix $\tilde{A}$. We apply their technique by using the similarity transformation $\bar{C} = T\bar{B}T^{-1}$ where

$$T = \begin{bmatrix} d_1 & d_1 & \ldots & d_1 \\ 0 & d_2 & \ldots & d_2 \\ \vdots & \ddots & \ddots & \vdots \\ 0 & \ldots & 0 & d_{N-1} \end{bmatrix}, \tag{77}$$

$d_i > 0$, $i = 1,\ldots,N-1$, and

$$T^{-1} = \begin{bmatrix} d_1^{-1} & -d_2^{-1} & 0 & \ldots & 0 \\ 0 & d_2^{-1} & -d_3^{-1} & \ldots & \vdots \\ \vdots & \ddots & \ddots & \ddots & 0 \\ \vdots & & \ddots & \ddots & -d_{N-1}^{-1} \\ 0 & \ldots & \ldots & 0 & d_{N-1}^{-1} \end{bmatrix}. \tag{78}$$

Granovsky and Zeifman proved a stronger result, but we note here that it is always possible to pick a sequence $d_1,\ldots,d_{N-1}$ so that $\bar{C} \in \mathscr{C}$. Column sums of $\bar{C}$ take the form

$$c_j = -a_j - b_{j+1} + \delta_j a_{j+1} + \delta_{j-1}^{-1} b_j \tag{79}$$

where

$$a_j = \frac{1}{N}(N-j)j,$$
$$b_j = \frac{1}{N}j(j-1)\tilde{\gamma}^{-1}, \tag{80}$$
$$\delta_j = \frac{d_{j+1}}{d_j}, \qquad j = 1 \ldots N-1.$$

Clearly, $a_N = b_1 = 0$. Picking

$$\delta_j = \frac{j}{j+2} \tag{81}$$

yields

$$c_1 = -\frac{N+1}{3N} - \frac{2}{\tilde{\gamma}N}$$

$$c_j = -\frac{(N+1)j}{N(j+2)}, \qquad j = 2, \ldots, N-2 \qquad (82)$$

$$c_{N-1} = -\frac{N-1}{N}.$$

The combination of (71) and (82) gives us a lower bound for the spectral gap $\beta_{\tilde{A}}$. That is,

$$\beta_{\tilde{A}} \geq \min\left\{\frac{N+1}{3N} + \frac{2}{\tilde{\gamma}N}, \frac{N+1}{2N}, \frac{N-1}{N}\right\} > \frac{1}{3}, \qquad \text{for } N > 1. \qquad (83)$$

Since $\tilde{\varepsilon} = O(1/N)$, we see that $\beta_{\tilde{A}} \gg \tilde{\varepsilon}$ if N is reasonably large. Since -1 is the nonzero eigenvalue of $\tilde{B}$ which is smallest in magnitude, this separates the time scales on which $\tilde{A}$ and $\tilde{\varepsilon}\tilde{B}$ affect the evolving probability distribution $\tilde{p}$ in (26), as desired.

4.2. **Spectral gap of an operator on ℓ^1.** To obtain a lower bound for the spectral gap of A in (6), we begin by deleting the first row and column as before. Next, we truncate A to be size $N \times N$. Then, we rewrite the system as in (75). Applying the same similarity transformation to this now-finite and transformed version of A, we get column sums of the form

$$c_{j,N} = -j - (j+1)j\gamma^{-1} + \delta_j(j+1) + \delta_{j-1}^{-1}j(j-1)\gamma^{-1}. \qquad (84)$$

Again, picking δ_j as in (81) and applying (71), we obtain a lower bound on the spectral gap for our modified version of A, call it β'_A. Indeed,

$$\beta'_A \geq \min\left\{\frac{1}{3} + 2\gamma^{-1}, \frac{1}{2}, N-1\right\}. \qquad (85)$$

Finally, we let $N \to \infty$ to obtain

$$\beta_A \geq \min\left\{\frac{1}{3} + 2\gamma^{-1}, \frac{1}{2}\right\}. \qquad (86)$$

We now see that the magnitude of the smallest eigenvalue for the operator A is $O(1)$, whereas since we can read the eigenvalues of B off its diagonal, its spectral gap is exactly 1. Hence, if n_S is large enough ε is small, and it is appropriate to treat A and εB as acting on different time scales as we have done in section 2.2.

5. **Discussion.** Keizer's paradox is that, for the simple autocatalytic reaction (1), the deterministic model based on the law of mass action has a nontrivial stable steady state to which all solutions with nonzero initial conditions tend, while the stochastic model of the same reaction predicts that extinction occurs with probability 1. This paradox is similar to a relatively simple example of a more general principle of a Markov process on a finite discrete state space, namely, that the system evolves to its absorbing states with probability 1. In the case of population dynamics, the only absorbing states are those for which the reproducing species is extinct. Thus, even though many deterministic models of reproducing populations predict long term persistence, stochastic models of these dynamical processes predict certain extinction.

The question of interest is, then, how long it takes before we can expect the stochasticity of the dynamics to bump the system to a state sufficiently far from the deterministic equilibrium that extinction occurs.

In this paper we find analytical estimates of the expected extinction times for two variations of an autocatalytic reaction. The first is an open system in which the substrate molecule S is held constant by some feedback mechanism, and the autocatalytic molecule X degrades at a constant rate. This stochastic model has an infinite state space, which makes numerical analysis of its (infinite) $\mathbb{W}$-matrix impossible. Through analysis of the relative spectral gaps of the operators formed by the transition rates from each of (1a) and (1b), we are able to justify the projection onto the nullspace of the operator A as an accurate approximation to the solution. This is because this nullspace is a slow manifold, provided $\varepsilon \ll 1/3$, and movement on this slow manifold gives an exponential waiting time for extinction. This nullspace is the span of the extinct distribution and a truncated Poisson distribution or quasistationary distribution. We find that the expected time to reach the mean of the quasistationary distribution from state 1 is very small compared to the massive waiting time to extinction.

The second variation is a closed system in which X does not degrade, but can convert back to S spontaneously. The absence of a feedback means the number of total molecules is conserved rather than the number of S molecules. Because this system is finite, we are able to compare the expected extinction time from state 1 with the exponentially large estimate from the reduction to a quasistationary distribution. From state 1, there is also a very high probability and a relatively small expected time to reach the mean of this distribution.

Thirdly, we are able to use the projection onto the nullspace of A to analyze the reaction with degradation in a closed environment. The disagreement between deterministic and stochastic models in this case is not whether the chemical species X goes extinct, but how much of the substrate S remains when extinction does occur. We find that our approximation from the nullspace projection above agrees well with distributions from Gillespie simulations, whereas the deterministic model does not predict even the mean of said distributions.

Finally, we consider a different, trimolecular reaction which exhibits the same paradox as the first two. Extinction time is more unwieldy to compute for this reaction, but we are able to obtain a similar prediction for the exit distribution of substrate molecules.

The resolution of Keizer's paradox, at least for the systems studied here, is that while extinction is certain, the expected time to extinction is exponentially large in the size of the system. We conjecture that the stochastic model for any system with similar paradoxical behavior, especially those biological systems which are observed to persist over long periods of time, has an extinction time which is exponentially large as a function of its characteristic population size.

REFERENCES

[1] L. J. S. Allen, "An Introduction to Stochastic Processes with Applications to Biology," Pearson Education, Inc., 2003.

[2] J. Beischke, P. Weber, N. Sarafoff, M. Beekes, A. Giese and H. Kretzschmar, *Autocatalytic self-propagation of misfolded prion protein*, Proc. Natl. Acad. Sci., **101** (2004), 12207–12211.

[3] C. W. Gardiner, "Handbook of Stochastic Methods. For Physics, Chemistry and the Natural Sciences," Second edition, Springer Series in Synergetics, **13**, Springer-Verlag, Berlin, 1985.

[4] B. L. Granovsky and A. I. Zeifman, *The decay function of nonhomogeneous birth-death processes, with application to mean-field models*, Stoch. Process. Appl., **72** (1997), 105–120.

[5] B. L. Granovsky and A. I. Zeifman, *The N-limit of spectral gap of a class of birth-death Markov chains*, Appl. Stoch. Models Bus. Ind., **16** (2000), 235–248.

[6] J. Keizer, "Statistical Thermodynamics of Nonequilibrium Processes," Springer-Verlag, 1987.

[7] T. G. Kurtz, *Limit theorems for sequences of jump Markov processes approximating ordinary differential processes*, J. Appl. Prob., **8** (1971), 344–356.

[8] T. G. Kurtz, *The relationship between stochastic and deterministic models for chemical reactions*, J. Chem. Phys., **57** (1972), 2976–2978.

[9] I. Nåsell, *Extinction and quasi-stationarity in the Verhulst logistic model*, Journal of Theoretical Biology, **211** (2001), 11–27.

[10] H. Qian and L. M. Bishop, *The chemical master equation approach to nonequilibrium steady-state of open biochemical systems: Linear single-molecule enzyme kinetics and nonlinear biochemical reaction networks*, Int. J. Mol. Sci., **11** (2010), 3472–3500.

[11] N. van Kampen, "Stochastic Processes in Physics and Chemistry," Lecture Notes in Mathematics, **888**, North-Holland Publishing Co., Amsterdam-New York, 1981.

[12] M. Vellela and H. Qian, *A quasistationary analysis of a stochastic chemical reaction: Keizer's paradox*, Bull. Math. Biol., **69** (2007), 1727–1746.

E-mail address: parker@math.utah.edu
E-mail address: keener@math.utah.edu

CHAPTER 4

THE BACTERIAL FLAGELLAR ROTARY MOTOR

Many bacterial species such as *E. coli* and *Salmonella* locomote by rotating helical flagella. Each bacterial cell has between three and eight flagella. When all the flagella rotate counterclockwise (CCW) they form a bundle behind the cell that propels the cell forward through its environment. If one or more of the flagella switches direction and rotates clockwise (CW), it causes the bundle to flay apart and the cell to rotate to a different orientation until all the flagella are once again simultaneously rotating CCW. This type of movement is commonly called a run-and-tumble process, and the frequency of tumbling is modified by the cell in response to environmental conditions such as nutrient or toxin gradients.

The flagellar rotation is driven by a complex transmembrane molecular machine appropriately called the flagellar rotary motor [2, 14]. Two major components constitute this motor: the rotor [10] and the stator. The rotor is the part of the complex that actually rotates and is directly attached to a hook from which the flagellum protrudes. It is comprised of several different rings, and each ring is made of many copies of different proteins. The stator is the portion of the motor that remains more or less stationary in the cell membrane. It is able to remain stationary by being embedded in the rigid peptidoglycan layer. The stator interacts with the high concentration of hydrogen ions in the periplasm to propel the rotor.

The exact mechanism of how the hydrogen ions cause motor rotation is not known. What is known is that they interact with the stator protein complex formed by MotA and MotB. This complex appears to interact with the protein FliG in the M ring which is part of the rotor. It also appears that the conformation of FliG determines whether the motor rotates CW or CCW at each of these interactions. How the conformation of FliG is decided is what we seek to understand in what follows.

FliG and the M ring is connected to the C ring, which is comprised of the proteins FliM and FliN, seen in Figure 4.1. The M ring and C ring make up what is called the switch complex. The chemotactic signaling molecule CheY can bind to FliN when it is in its phosphorylated form, CheY-P [12]. When the whole complex composed of FliN, FliM, and FliG has CheY-P bound it is biased toward its CW conformation [8, 9]. There is a 26-fold rotational symmetry in the M ring and an apparent 34-fold rotational symmetry in the C ring. It is not known whether this stoichiometric
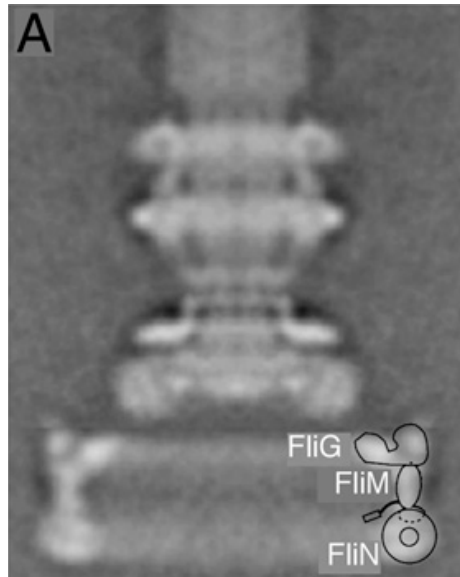
Figure 4.1. The flagellar rotor. An electron microscopic image of the flagellar rotor in *Salmonella*. (Adapted from [12].)

mismatch is important for motor control. For our purposes, we do not consider the 26-fold symmetry created by FliG explicitly.

In short, our aim is to develop a tractable model of the overall conformation of the switch complex based on simple assumptions about the interaction of the individual components involved.

4.1   Model of the Flagellar Motor Switch

The initial framework of the stochastic model of this motor, described in the following, is the same as the model that was proposed by Bai et al. [1]. We consider a ring of subunits, each of which can exist in one of four states. A subunit can have CheY-P bound or unbound, and it can be in one of two conformations which we will call CCW and CW. As mentioned above, the CCW and CW conformations for individual subunits at this point are only conformations. The actual direction of rotation of the motor is presumed to be a result of the aggregate of conformations of all subunits.

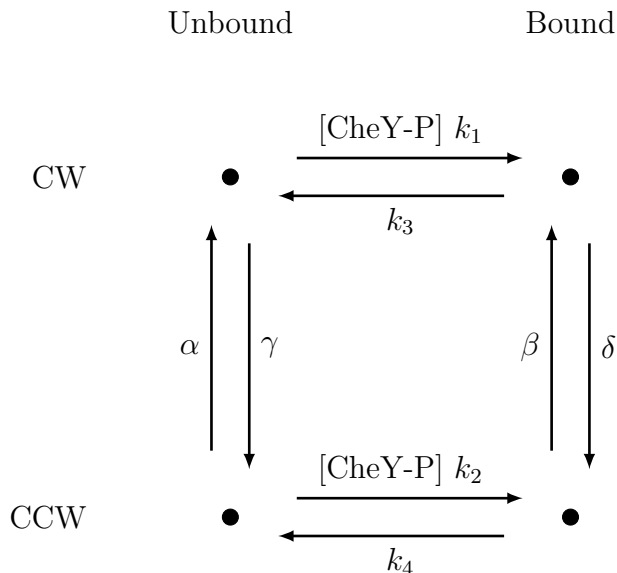These states and the transitions between them are represented in Figure 4.2.

Unbound   Bound

CW

[CheY-P] k_1

k_3

α γ β δ

[CheY-P] k_2

CCW

k_4

Figure 4.2. State diagram for a single subunit with four states. Transition diagram for a single subunit in the ring of proteins that constitute the flagellar switch. The rates in this diagram are state-dependent. Specifically, we use the switching rates α, β, γ, and δ to mean the unbiased switching rate of a subunit, or the switching rate of a subunit whose two nearest neighbors are in opposite conformations. We make the assumption for the sake of simplicity that the conformations of neighboring subunits influence the switching rates of a subunit symmetrically and equally in both directions. That is, for some $\omega > 1$, if both nearest neighbors of a subunit are CW, then, in our model, the rates for that subunit to switch from CCW to CW are $\omega\alpha$ and $\omega\beta$, and the rates for it to switch from CW to CCW are $\frac{1}{\omega}\gamma$ and $\frac{1}{\omega}\delta$ depending on if it has CheY-P bound or not. Likewise, if its nearest neighbors are both CCW, then the CW switching rates are $\frac{1}{\omega}\alpha$ and $\frac{1}{\omega}\beta$, and the CCW switching rates are $\omega\gamma$ and $\omega\delta$. We call ω the coupling strength since it indicates how strongly the conformations of neighboring subunits are coupled.

4.1.1 An Early Attempt at Model Reduction

Since there are 34 subunits in this ring, this stochastic process is a Markov process on a state space with 4^{34} states. To attempt to compute the stationary distribution on this state space would require an immense matrix calculation. However, we don't need the stationary distribution on the full state space. We are only interested in the expected proportion of subunits that are CW for a given concentration of cytoplasmic CheY-P. Therefore, we can think of this as a stochastic process on a state space with only 35 states, as shown in Figure 4.3. In order to do anything with this model, we must relate the g_i's and r_i's in Figure 4.3 to the parameters in the full 4^{34}-state
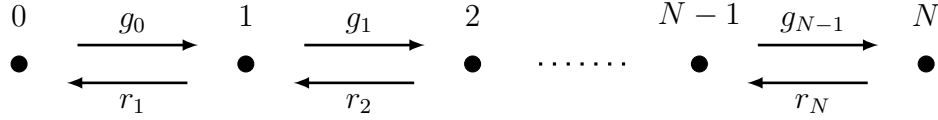
Figure 4.3. State space diagram with 35 states. Diagram representing the number of CW subunits.

system.

One idea is to use the proportion of CCW and CW subunits as weighting factors for the CW, CCW switching rates in Figure 4.2. Additionally, since the CheY-P binding and unbinding rates are independent of nearest neighbor relationships, we can treat the probability that a subunit has CheY-P bound independently and in equilibrium, conditional only upon whether it is, itself, in the CW or CCW conformation. Thus, we define

$$p_{u|\text{CW}} = \frac{k_3}{[\text{CheY-P}]k_1 + k_3},\tag{4.1}$$

$$p_{b|\text{CW}} = 1 - p_{u|\text{CW}},\tag{4.2}$$

$$p_{u|\text{CCW}} = \frac{k_4}{[\text{CheY-P}]k_2 + k_4}, \quad \text{and}\tag{4.3}$$

$$p_{b|\text{CCW}} = 1 - p_{u|\text{CCW}}.\tag{4.4}$$

This produces the following hypothesis for effective transition rates:

$$g_n = (N - n)\left(p_{u|\text{CCW}}\,\alpha + p_{b|\text{CCW}}\,\beta\right)\phi_n, \qquad n = 0, 1, \ldots, N - 1\tag{4.5}$$

$$r_n = n\left(p_{u|\text{CW}}\,\gamma + p_{b|\text{CW}}\,\delta\right)\psi_n, \qquad n = 1, 2, \ldots, N\tag{4.6}$$

where

$$\phi_n = \frac{1}{\omega}\frac{(N - 1 - n)(N - 2 - n)}{(N - 1)(N - 2)} + 2\frac{(N - 1 - n)\,n}{(N - 1)(N - 2)} + \omega\frac{n\,(n - 1)}{(N - 1)(N - 2)}\tag{4.7}$$

and

$$\psi_n = \frac{1}{\omega}\frac{(N - n)(N - n - 1)}{(N - 1)(N - 2)} + 2\frac{(N - n)(n - 1)}{(N - 1)(N - 2)} + \omega\frac{(n - 1)(n - 2)}{(N - 1)(N - 2)}\tag{4.8}$$

are the average biases for conformation switching, weighted by the proportions of possible neighbors.

With this hypothesis for appropriate g_i's and r_i's, we can look at the steady state distribution for the process shown in Figure 4.3. This equilibrium distribution

depends, of course, on all the rates shown and described in Figure 4.2, and two of those rates depend linearly on [CheY-P]. For a first pass glance at this distribution, we simply choose the rates found by Bai et al. as shown in Figure 4.4 and allow [CheY-P] (called $c/c_{0.5}$ in their work) to vary over the same range as they did [1]. We compare distributions of time spent in states with a given number of CW subunits over the course of several stochastic simulations, shown in Figure 4.5, to these distributions from our reduction, shown in Figure 4.6.

A glance at Figure 4.6 is enough to see that these sets of distributions look nothing like Figure 4.5. Our hypothesis for state transition rates given by (4.5) and (4.6) must not have been an appropriate guess. What went wrong? What rates shall we choose in order to reduce the number of states in our prodigious system?

The answer to the question of why this reduction does not give similar results to stochastic simulations lies in the way we have probabilistically chosen nearest neighbor interactions. By using the frequencies of appearance of CW versus CCW subunits we have, in essence, homogenized the ring so that each subunit's two nearest
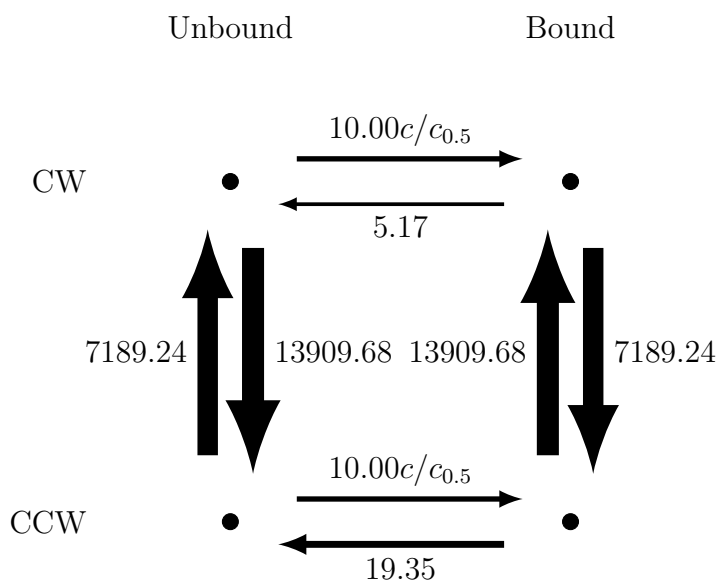

Figure 4.4. Parameters from Bai et al. Diagram representing parameters from [1]. Arrow widths have been scaled like the log of each rate for quick visual reference. The other parameter not pictured in the diagram is the neighbor coupling strength, $\omega = 62.18$, which scales the vertical arrows in this diagram depending on the states of the two nearest neighboring subunits.
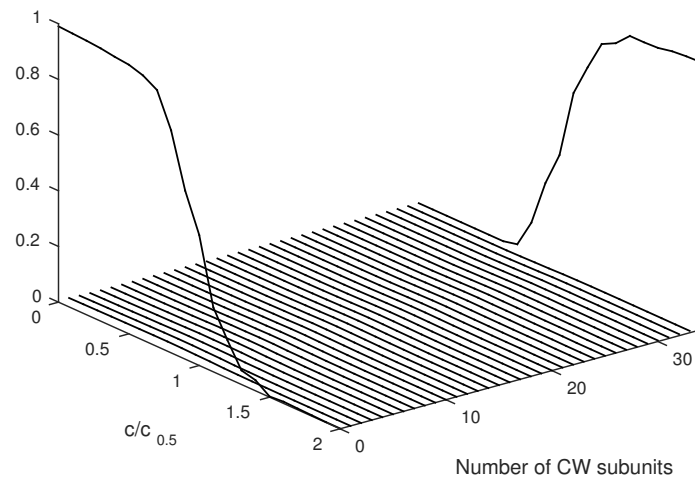
Figure 4.5. Simulated distributions as a function of $c/c_{0.5}$. The fraction of time spent in each state with a given number of CW subunits $(0, \dots, 34)$ over the course of stochastic simulations for $c/c_{0.5}$ ranging between $[0, 2]$. Parameters are chosen as shown in Figure 4.4.
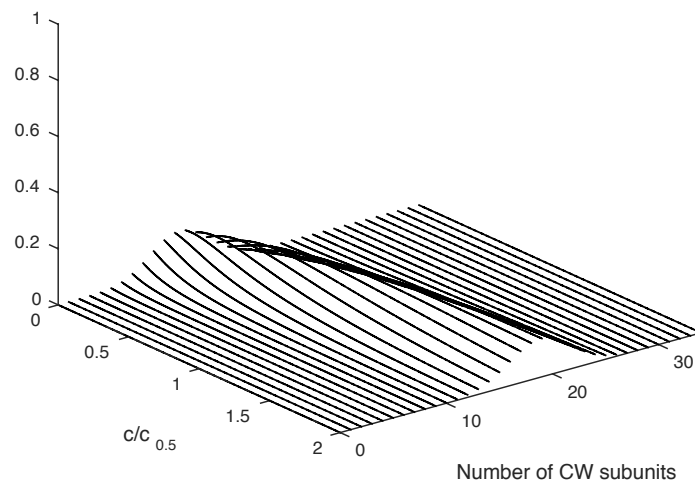

Figure 4.6. Stationary distribution on 35 states with homogenized transition rates. Stationary distributions of the reduction to the process shown in Figure 4.3 with rates as described by (4.5),(4.6). Parameters are chosen as shown in Figure 4.4.

neighbors can be in either conformation as if the system is well-mixed. This is like dumping several blue balls into an urn, then dumping several red balls into the same urn, and, without any shaking or mixing, picking one off the top. The probability that the chosen ball is red is not simply a function of the number of each color of ball in the urn. The homogenized model we have guessed at here is similar in some ways to a mean field model. It accounts for bias in conformational switching, but in a smoothed-out way that partially ignores the very important energetic neighbor-neighbor interactions. We try a different reduction in what follows.

4.1.2   Better Model Reduction

Because the conformational switching rates of subunits is strongly biased by the conformation of its two nearest neighbors, as has been observed in simulations [5, 1, 7], conformational spread is the primary mode for the entire ring to switch from all subunits in one conformation to all subunits in the opposite conformation, either all CCW to all CW or vice versa. That is, most often this complete switching occurs by a connected domain of subunits growing to neighboring subunits until the domain has spread around the entire ring.

We approximate the full Markov process by making the, as yet, unjustified, assumption that the ring of subunits can only have at most two domains: one set of contiguous subunits that are all CCW and that the rest of the subunits (a necessarily connected set) are in the CW conformation. Hence, if there are two domains present at a given time, only four subunits are able to switch conformation, those four in the ring whose two nearest neighbors are in opposite conformations. If all subunits are in the same conformation, however, any one of the 34 may switch conformation.

This restriction on the full process reduces the size of the state space a great deal. We essentially ignore all states with more than one domain of CW subunits while still hoping to capture the dynamics that invoke the entire ring of subunits to switch conformation. A schematic of the types of transitions we are eliminating is shown in Figure 4.7

With this in mind, we retain the quasistationary state approximation for CheY-P binding to subunits as in (4.1)-(4.4). That is, we take the probability that each subunit
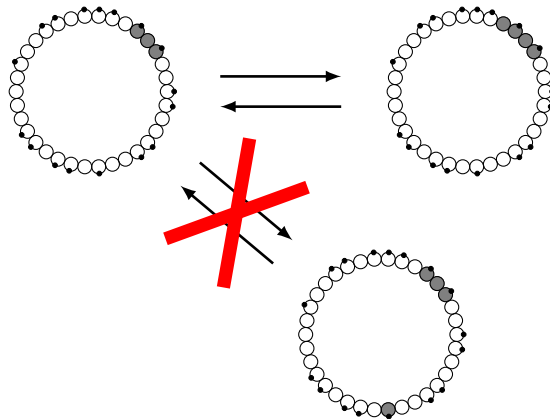
Figure 4.7. Eliminated states and transitions. A schematic of one allowed and one disallowed transition and state from the state space after reducing using the 2-domain assumption described. Unshaded circles represent CCW subunits, and shaded represent CW. The small black circles on the edge of some of the bigger circles represent bound CheY-P. We do not explicitly track which subunits have CheY-P bound and which do not.

has CheY-P bound to be in steady state given its particular conformation. Such an approximation here may seem to imply that the binding reaction is fast compared to the conformational switching. If the binding reaction is, indeed, much faster, then the approximation is certainly justifiable. However, in this case, as one edge of a domain of CW subunits moves around the ring, it encounters several subunits, each of which may have CheY-P bound or not. The fraction of subunits that have CheY-P bound is the average we aim to capture with this quasistationary state approximation. Using this fraction allows us to compute the average rate at which the edge of the domain moves around the ring.

With this quasi-equilibrium and the restriction to one domain of subunits of each conformation we have, once again, reduced the full process to a process on 35 effective states as shown in Figure 4.3. Each state still represents the number of subunits in the CW conformation. We must now select the appropriate g_i's and r_i's.

First, we consider g_0. It is the rate at which any one of the subunits in a ring of all CCW subunits switches conformation to CW. Taking into account the equilibrium distribution regarding binding, we find that

$$g_0 = \frac{N}{\omega} \left(\alpha \, p_{u \mid CCW} + \beta \, p_{b \mid CCW} \right).$$

(4.9)

The factor of N in this rate comes from the fact that any one of the subunits can switch when all are in the same conformation, and the $\frac{1}{\omega}$ comes from the fact that if all subunits are CCW, then the two nearest neighbors of any subunit are, necessarily, both CCW. However, once a single subunit is in the CW conformation, in order to get two CW subunits, we only consider the rate at which one of the neighbors of the first subunit switches. Since its two nearest neighbors are in opposite conformations,

$$g_1 = 2 \left(\alpha \, p_{u|CCW} + \beta \, p_{b|CCW} \right). \tag{4.10}$$

In fact, $g_i = g_1$ for $i = 2, \ldots, N-2$. We call this rate g_n. To compute g_{N-1} we note that if every subunit but one is CW, then both neighbors of the only remaining CCW subunit are CW. Therefore,

$$g_{N-1} = \omega \left(\alpha \, p_{u|CCW} + \beta \, p_{b|CCW} \right). \tag{4.11}$$

Similarly,

$$r_1 = \omega \left(\gamma \, p_{u|CW} + \delta \, p_{b|CW} \right), \tag{4.12}$$

$$r_n = r_i = 2 \left(\gamma \, p_{u|CW} + \delta \, p_{b|CW} \right), \quad i = 2, \ldots, N-1, \tag{4.13}$$

and

$$r_N = \frac{N}{\omega} \left(\gamma \, p_{u|CW} + \delta \, p_{b|CW} \right). \tag{4.14}$$

With this new, and hopefully improved, set of g_i's and r_i's, we look, again, at the steady state distribution for the process shown in Figure 4.3. Using the same range for $c/c_{0.5}$, these distributions are shown in Figure 4.8. We have imposed data points for the end states, 0 and N, from the simulations in Figure 4.5 onto the distributions predicted by our improved, reduced model. It is worth noting here that the distributions in Figure 4.5 include time spent in *all* states visited during the simulations, regardless of the number of CW and CCW domains in the ring of subunits. The remarkable agreement between Figures 4.8 and 4.5 suggests that the reduction to 35 states simply by neglecting the contributions of states with more than two domains captures the major features of the dynamics of the whole process.
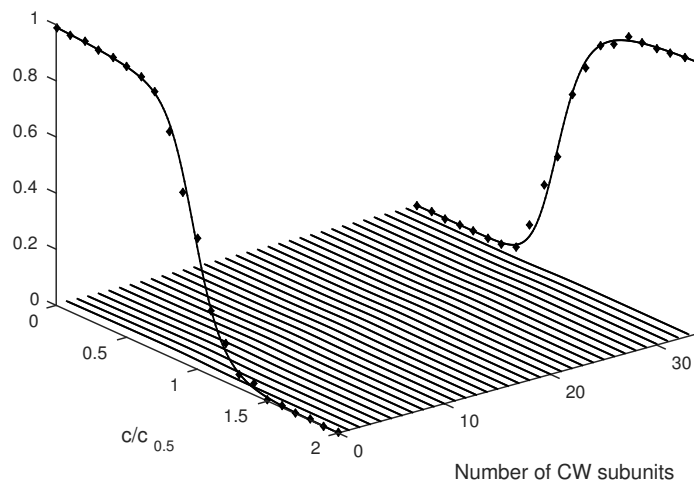
Figure 4.8. Stationary distributions on 35 states as a function of $c/c_{0.5}$ with simulated data imposed. Stationary distributions on the number of CW subunits with the reduction to rates shown in Figure 4.3 given by (4.9)-(4.14). Data from the end states in Figure 4.5 is imposed here for comparison. Parameters are, again, chosen as shown in Figure 4.4.

4.2   Further Model Reduction

Our key observation about both of these distributions is that they are heavily weighted on the ends. That is, the process spends almost all of its time with either none or all of the subunits in the CW state. In fact, by taking the $-\log$ of the distributions in Figure 4.8, we plot what can be interpreted as an energy potential in Figure 4.9. We see in this plot that the two end states, 0 and 34, are like low energy potential wells compared to the relatively high energy interior states. We also see the bias toward one end state or the other as a continuously varying function of $c/c_{0.5}$.

This observation seems to indicate that, once again, we can reduce the number of states we need to consider in order to answer questions about the overall dynamics of this process. This same observation holds for every set of rate parameters we have used to create such plots as long as $\omega \gg 1$. In other words, the coupling strength between nearest neighbors must be relatively strong, lowering the energy threshold for conformation switching by a few $k_B T$. With this stipulation we can now reduce
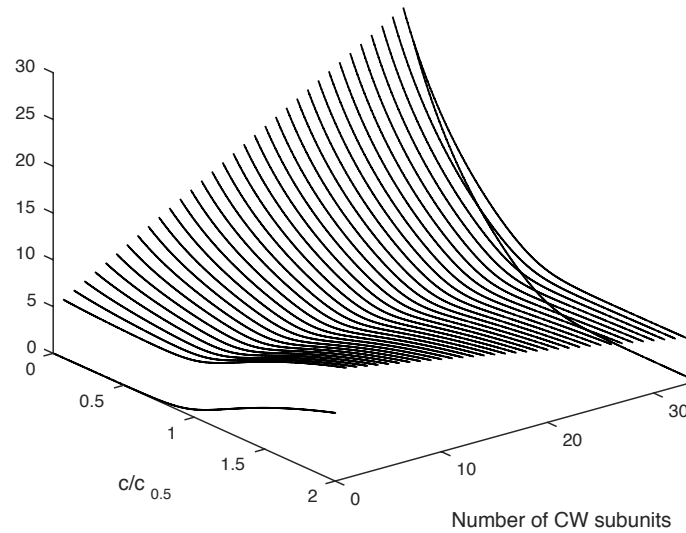
Figure 4.9. Energy potentials from stationary distributions. Energy potentials for the process with stationary distributions as in Figure 4.8.

the number of effective states from 35 to just 2 as in Figure 4.10. The rates g and r must be appropriate effective rates of moving from one end state to the other in Figure 4.3. In other words, they should be the respective inverses of the mean first passage times $T_{N,0}$ and $T_{0,N}$, where $T_{j,i}$ is the expected first time for the process to arrive at state j having started at state i.

There is a convenient method to compute splitting probabilities as well as first passage times for continuous time, discrete state Markov chains. At this point, we don't need any splitting probabilities, so we focus on the mean first passage times. Define $\mathbf{q}$ to be the vector of probabilities for all absorbing states. In our case, to obtain $T_{j,i}$, we first treat only the boundary state j to be absorbing because we are interested in the first time to arrive at state j. Define $\mathbf{p}$ to be the vector of probabilities of all
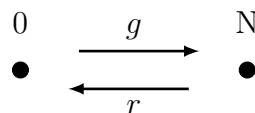

Figure 4.10. State space diagram for the entire switch reduced to two states. Reduction of the diagram in Figure 4.3.

nonabsorbing states. Then,

$$\frac{d\mathbf{p}}{dt} = \mathbf{A}\mathbf{p}$$
$$\frac{d\mathbf{q}}{dt} = \mathbf{B}\mathbf{p}, \tag{4.15}$$

where $\mathbf{A}$ is the matrix describing transitions between and out of all states represented by the probabilities in $\mathbf{p}$ and $\mathbf{B}$ is the (strictly nonnegative) matrix of rates into states represented by the probabilities in $\mathbf{q}$. $\mathbf{A}$ is necessarily invertible since any nonzero entries in the solution of $\mathbf{A}\mathbf{p} = \mathbf{0}$ would correspond to absorbing states and should be included in $\mathbf{q}$. Since entries of $\mathbf{q}(t)$ are probabilities for any $t \geq 0$, entries of $\dfrac{d\mathbf{q}}{dt}$ are probability densities. Hence, the vector of expected times to arrive at a state in $\mathbf{q}$ from an initial distribution $\mathbf{p}(0)$ is

$$
\begin{aligned}
\mathbf{T} &= \int_0^\infty t\,\frac{d\mathbf{q}}{dt}\,dt \\
&= \int_0^\infty t\,\mathbf{B}\mathbf{p}\,dt \\
&= \mathbf{B}\int_0^\infty t\,\mathbf{A}^{-1}\frac{d\mathbf{p}}{dt}\,dt \\
&= \mathbf{B}\mathbf{A}^{-1}\left([t\mathbf{p}]_0^\infty - \int_0^\infty \mathbf{p}\,dt\right) \\
&= -\mathbf{B}\mathbf{A}^{-2}\int_0^\infty \frac{d\mathbf{p}}{dt}\,dt \\
&= -\mathbf{B}\mathbf{A}^{-2}\left(\mathbf{p}(\infty) - \mathbf{p}(0)\right) \\
&= \mathbf{B}\mathbf{A}^{-2}\mathbf{p}(0).
\end{aligned}
\tag{4.16}
$$

In our case, to compute $T_{N,0}$, we let $\mathbf{q} = (p_N)$. Thus, $\mathbf{p}$ is the vector containing the probabilities of all the other states,

$$\mathbf{p} = \begin{pmatrix} p_0 \\ p_1 \\ \vdots \\ p_{N-1} \end{pmatrix}. \tag{4.17}$$

The corresponding matrices are the tridiagonal

$$\mathbf{A} = \begin{pmatrix} -g_0 & r_1 & & & & & \\ g_0 & -(r_1 + g_n) & r_n & & & & \\ & g_n & -(r_n + g_n) & r_n & & & \\ & & \ddots & \ddots & \ddots & & \\ & & & g_n & -(r_n + g_n) & r_n & \\ & & & & g_n & -(r_n + g_{N-1}) & \end{pmatrix} \tag{4.18}$$

and the $1 \times N$

$$\mathbf{B} = \begin{pmatrix} 0 & \cdots & 0 & g_{N-1} \end{pmatrix}. \tag{4.19}$$

The rate r_N does not appear in either $\mathbf{A}$ or $\mathbf{B}$ because we are not considering escape from state N. $T_{N,0}$ is simply the first exit time to the right boundary with the left boundary reflecting.

$\mathbf{A}^{-1}$ is cumbersome to compute analytically, however, we do not need it to obtain $T_{N,0}$. We compute $T_{N,0}$ by noticing that

$$T_{N,0} = \mathbf{B}\mathbf{y} \tag{4.20}$$

where

$$\mathbf{A}\mathbf{y} = \mathbf{x} \tag{4.21}$$

and

$$\mathbf{A}\mathbf{x} = \mathbf{p}(0). \tag{4.22}$$

Since the initial condition is the simple $\mathbf{p}(0) = \begin{pmatrix} 1 \\ 0 \\ \vdots \\ 0 \end{pmatrix}$, we can backsolve both of these equations analytically. Keeping with the convention that the indices of entries of $\mathbf{x}$ and $\mathbf{y}$ range from 0 to $N - 1$, we see that for $j = 2, \ldots, N - 2$,

$$g_n x_{j-1} - (r_n + g_n) x_j + r_n x_{j+1} = 0. \tag{4.23}$$

Guessing a solution of the form $x_j = \mu^j$ for $j = 1, \ldots N - 1$ yields the quadratic equation

$$g_n - (r_n + g_n) \mu + r_n \mu^2 = 0 \tag{4.24}$$

which has two solutions, $\mu = 1, \frac{g_n}{r_n}$. For convenience, we define $\lambda = \frac{g_n}{r_n}$. The linearity of this equation allows the general solution $x_j = A\lambda^j + B$. The remaining three equations to satisfy are

$$-g_0\, x_0 + r_1 \left(A\lambda + B\right) = 1, \tag{4.25}$$

$$g_0\, x_0 - \left(r_1 + g_n\right)\left(A\lambda + B\right) + r_n\left(A\lambda^2 + B\right) = 0, \tag{4.26}$$

$$g_n\left(A\lambda^{N-2} + B\right) - \left(r_n + g_{N-1}\right)\left(A\lambda^{N-1} + B\right) = 0. \tag{4.27}$$

From (4.25) we get $g_0\, x_0 = r_1\left(A\lambda + B\right) - 1$, so

$$\begin{pmatrix} 0 & -g_n + r_n \\ -g_{N-1}\lambda^{N-1} & g_n - r_n - g_{N-1} \end{pmatrix} \begin{pmatrix} A \\ B \end{pmatrix} = \begin{pmatrix} 1 \\ 0 \end{pmatrix}. \tag{4.28}$$

Hence by inverting the matrix on the LHS of this equation, we get

$$\begin{pmatrix} A \\ B \end{pmatrix} = \frac{1}{(r_n - g_n)g_{N-1}\lambda^{N-1}} \begin{pmatrix} g_n - r_n - g_{N-1} \\ g_{N-1}\lambda^{N-1} \end{pmatrix}, \tag{4.29}$$

and

$$g_0\, x_0 = \frac{r_1(g_n - r_n - g_{N-1})\lambda + (r_n - g_n - r_1)g_{N-1}\lambda^{N-1}}{(r_n - g_n)g_{N-1}\lambda^{N-1}}. \tag{4.30}$$

Now that we know the RHS of (4.21) we can solve for $\mathbf{y}$. Again, for $j = 1, \ldots, N-1$, we guess a solution. Since $C\lambda^j + D$ spans the nullspace of the second-order difference equation (4.23), we try a particular solution of the form $y_j = C\lambda^j + D + j(E\lambda^j + F)$. This guess is a solution if

$$-g_n E\lambda^{j-1} + r_n E\lambda^{j+1} = A\lambda^j \tag{4.31}$$

$$\implies E = \frac{A\lambda}{g_n(\lambda - 1)}, \tag{4.32}$$

and

$$-g_n F + r_n F = B \tag{4.33}$$

$$\implies F = \frac{B\lambda}{g_n(1 - \lambda)}. \tag{4.34}$$

Once again, y_0, C and D are obtained by satisfying the remaining three equations,

$$-g_0 \, y_0 + r_1 \left(C\lambda + D + E\lambda + F\right) = \frac{1}{g_0} \left(r_1(A\lambda + B) - 1\right) \tag{4.35}$$

$$g_0 \, y_0 - (r_1 + g_n) \left(C\lambda + D + E\lambda + F\right) + r_n \left(C\lambda^2 + D + 2E\lambda^2 + 2F\right) = A\lambda + B \tag{4.36}$$

$$g_n \left(C\lambda^{N-2} + D + (N-2)E\lambda^{N-2} + (N-2)F\right)$$
$$- (r_n + g_{N-1}) \left(C\lambda^{N-1} + D + (N-1)E\lambda^{N-1} + (N-1)F\right) = A\lambda^{N-1} + B. \tag{4.37}$$

Solving for $g_0 \, y_0$ in (4.35) and substituting into (4.36), we obtain the matrix equation

$$\begin{pmatrix} 0 & -g_n + r_n \\ -g_{N-1}\lambda^{N-1} & g_n - r_n - g_{N-1} \end{pmatrix} \begin{pmatrix} C \\ D \end{pmatrix} = \begin{pmatrix} G \\ H \end{pmatrix}. \tag{4.38}$$

which is the same as (4.28), but with a different RHS.

$$G = \frac{1}{g_0}(r_1(A\lambda + B) - 1) + g_n(E\lambda + F) - 2r_n(E\lambda^2 + F) + A\lambda + B \tag{4.39}$$

and

$$H = -g_n(N-2)(E\lambda^{N-2} + F) + (r_n + g_{N-1})(N-1)(E\lambda^{N-1} + F) + A\lambda^{N-1} + B. \tag{4.40}$$

We solve for C and D by, again, multiplying by the appropriate inverse matrix to get

$$\begin{pmatrix} C \\ D \end{pmatrix} = \frac{1}{(r_n - g_n)g_{N-1}\lambda^{N-1}} \begin{pmatrix} g_n - r_n - g_{N-1} & g_n - r_n \\ g_{N-1}\lambda^{N-1} & 0 \end{pmatrix} \begin{pmatrix} G \\ H \end{pmatrix}. \tag{4.41}$$

Putting this all together gives

$$\begin{aligned}
T_{N,0} &= g_{N-1}y_{N-1} \\
&= g_{N-1} \left(C\lambda^{N-1} + D + (N-1)(E\lambda^{N-1} + F)\right) \\
&= \frac{1}{g_0 g_n g_{N-1}(\lambda - 1)^3} \left[g_n \left(r_1\lambda^{2-N}(\lambda - 1)^3 + g_0(\lambda - \lambda^{2-N})(\lambda - 1)^2\right) \right. \\
&\quad + g_{N-1} \left(g_n(\lambda - 1)^3 + \left(r_1(1 - \lambda^{2-N}) + g_0(N - 1)\right)\lambda(\lambda - 1)^2 \right. \\
&\qquad \left. \left. - g_0(\lambda - 1)(\lambda^2 - \lambda^{3-N})\right)\right].
\end{aligned} \tag{4.42}$$

We can compute $T_{0,N}$ the same way by letting state 0 be absorbing and state N be reflecting with initial condition $p_i(0) = \delta_{iN}$, or we can simply make appropriate

substitutions in the above expression, namely $g_{N-1} \leftrightarrow r_1$, $g_0 \to r_N$, $g_n \leftrightarrow r_n$ and $\lambda \to \lambda^{-1}$. We get

$$
\begin{aligned}
T_{0,N} = \frac{1}{r_1 g_n r_n (1-\lambda)^3} \Big[& g_n \left(g_{N-1} \lambda^{N-2} (1-\lambda)^3 + r_n (\lambda - \lambda^N)(1-\lambda)^2 \right) \\
& r_1 \left(g_n (1-\lambda)^3 + \left(g_{N-1}(1-\lambda^{N-2}) + r_N (N-1) \right) \lambda (1-\lambda)^2 \right. \\
& \left. - r_N (1-\lambda)(\lambda - \lambda^N) \right) \Big].
\end{aligned} \tag{4.43}
$$

In steady state, the process shown in Figure 4.10 with $g = 1/T_{N,0}$ and $r = 1/T_{0,N}$ has the distribution

$$
p_0 = \frac{T_{N,0}}{T_{N,0} + T_{0,N}}, \qquad p_N = \frac{T_{0,N}}{T_{N,0} + T_{0,N}}. \tag{4.44}
$$

This formula may look big and messy once the appropriate substitutions are made, but it is analytic, and it is derived directly from assumptions about the mechanism responsible for motor direction switching. Hence, without resorting to a Hill function, which is entirely phenomenological, we have a possible explanation for the high degree of cooperativity seen in the CW bias curve. Without altering parameters from those in Figure 4.4, we compare this steady state distribution with the distribution shown in Figure 4.8 as a function of $c/c_{0.5}$. This comparison is shown in Figure 4.11.

We would not expect the green and red curves in Figure 4.11 to match exactly unless the total steady state probability of being at any interior state in the 35-state model were exactly zero. However, qualitatively it is a good match, and, scaled appropriately, it is almost exact. It is also worth mentioning that the actual observed rotational behavior of the motor is unknown when the process is at any one of the interior states. Most models assume the velocity of the motor is a linear function of the number of CW units. Thus, the reduction to two states may, in fact, be quantitatively accurate depending on the motor behavior on the interior of the state space from Figure 4.3 [15].

Before proceeding any further, we can use this two-state reduction to point out an important feature of this motor. It is that the relatively large number of subunits in the ring of the switching mechanism is one of the primary factors in determining the degree of cooperativity in the CW bias curve. Plotted in Figure 4.12 are the CW bias curves predicted by the stationary distribution (4.44) for N ranging from 2 to 34
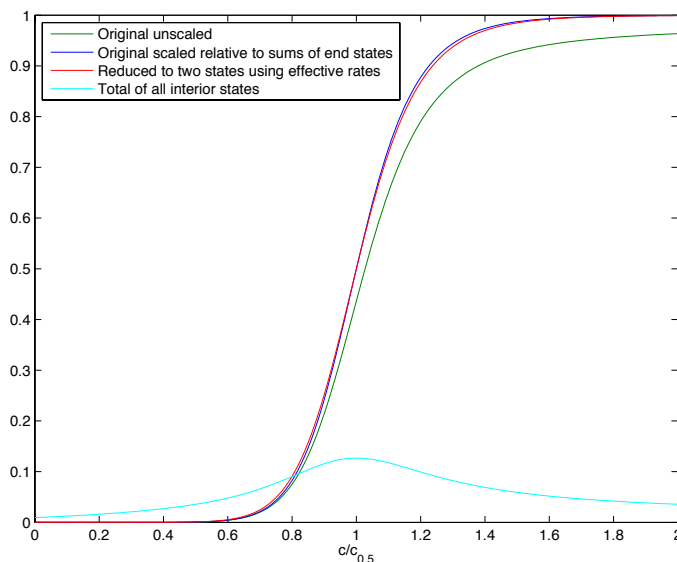
Figure 4.11. Stationary distribution on two states compared to end states of 35. The green curve is the same as the curve over state 34 in Figure 4.8. The red curve is p_N using the expressions (4.42) and (4.43). The blue curve is simply the green curve scaled by the sum of both end state probabilities in Figure 4.8. The cyan curve is the sum of the probabilities of all interior states in Figure 4.8. Since the cyan curve is not exactly zero for all values of $c/c_{0.5}$ there is a discrepancy between the green and blue curves.

with the same parameters used for all figures up to this point. We see that for smaller subunit numbers the CW bias curve becomes less and less cooperative (black to red). There is evidence that this motor has the capacity for dynamic subunit exchange from the cytosol [4, 16, 6]. It is unknown how this exchange is regulated or whether this is a mechanism to help the cell adapt its locomotion.

4.2.1 Parameter Estimation

We are particularly interested to see whether this model is capable of reproducing all the phenomena known about motor switching, and, if so, whether it can provide insight into the underlying parameters governing the behavior of each subunit. To this end we have obtained data from various sources. Cluzel et al. measured the CW bias, or, in other words, the percentage of time the motor spends rotating clockwise, as a function of the cytosolic CheY-P concentration [3]. They found the CW bias curve to be highly cooperative. They fit a Hill function to their data, yielding a Hill
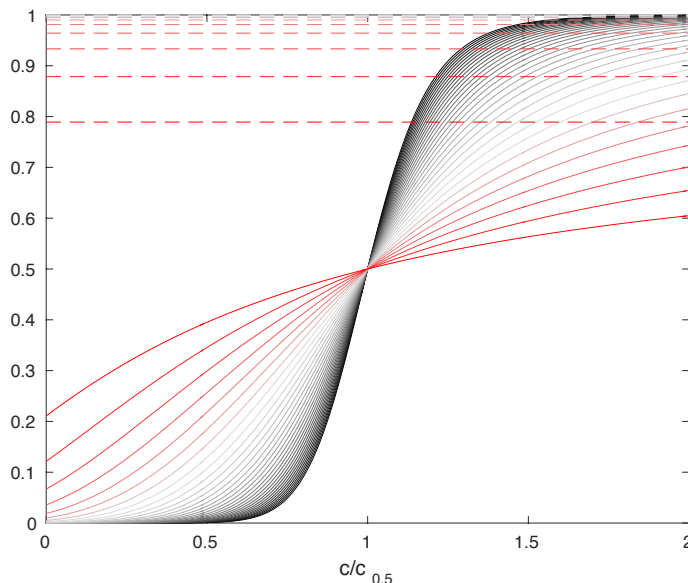
Figure 4.12. Stationary distribution on two states for a range of N. CW bias curves as predicted by the stationary distribution (4.44) for N ranging from 2 to 34 (red to black solid curves). Dashed lines are the asymptotic values for the CW bias as $c/c_{0.5} \to \infty$.

coefficient of 10.3 ± 1.1.

They also measured the average motor switching frequency using the same recordings. It is perhaps not surprising that for values of CheY-P that correspond to CW bias values very near 0 or 1, the switching frequency is essentially zero. For the small range of CheY-P values that yield intermediate CW bias values the switching frequency lies somewhere between 0 and 1.5 s^{-1}.

The other data we compare our model results with comes from Sourjik et al. [13]. They measured the fractional CheY-P occupancy. That is, given a cytoplasmic CheY-P concentration they were able to measure the fraction of FliM subunits that had a CheY-P molecule bound. They found that fitting a Hill function to this data gave a Hill coefficient of 1.7 ± 0.3. Hence, the binding of CheY-P to FliM appears to be much less cooperative than the conformation switching. More specifically, the binding and unbinding rates appear to be unaffected by the binding state of neighboring subunits or the CW/CCW conformation of the subunit.

One caveat about their data is that they were unable to distinguish between FliM

incorporated in fully formed motors and FliM in solution in the cell. The fractional CheY-P occupancy may feasibly be different between these two populations. However, we are still interested to see if the model can produce a lack of cooperativity in binding while retaining the high degree of cooperativity in the CW bias. Further support for this idea comes from Sagi et al. [11] They simultaneously and independently found a lack of cooperativity in the binding curve, though they used different experimental methods and their data has different units.

4.2.2 Fitting Method

We use the built-in MATLAB tool `lsqcurvefit`. We use the equilibrium value of p_N from the 2-state reduction above to fit the CW bias data. To fit the switching frequency data we use the inverse of the average of the two expected switching times; explicitly, $2/(T_{N,0} + T_{0,N})$. The fractional occupancy data requires a little bit more computation. Using the stationary distribution on the 35-state model, we take into account the probability that each subunit has CheY-P bound in each of the 35 states and sum appropriately to get an expected number of bound CheY-P at each concentration.

There is one other interesting issue to note before we begin fitting the data. Though the CW bias data and fractional occupancy have similar units, that is, they are each proportions ranging between 0 and 1 and are thus unitless, they were measured using different methods and describe qualitatively different objects. Thus, there may be more noise in one or the other. Whether the noise comes from experimental methods or is inherent in the processes measured or something else, we cannot compare them directly and cannot automatically assume that a data point from one set is equally valuable or important as a data point from the other set. Furthermore, the switching frequency data has different units entirely, and also cannot be directly compared with the other two. Nevertheless, we wish to use all available data to fit our model.

For this reason, a residual function for model fitting is somewhat ad hoc. The scale for each data set is arbitrary, so we try several options for weighting each set more or less heavily to see what gives us the "best" fit. As a first pass we try fitting

the raw data sets without any artificial weighting. The results of this parameter fit are represented in Figure 4.13. The first thing to notice about this parameter fit is that it seems to indicate that conformation switching is much slower when CheY-P is bound to the subunit. It is possible that, in addition to biasing a subunit toward the CW conformation, the binding of CheY-P does, in fact, slow down the conformation change rate as part of the mechanism for motor direction switching. However, this parameter fit is not unique. Parameter fitting sets vary quite widely, depending on the nucleation set, without much variation in the norm of the residual function. Figure 4.13 is one particular instance of the output from the fitting algorithm.

Because the CW bias data and the CheY-P occupancy data appear to be much less noisy than the switching frequency data, we try a fit giving both of these data sets more weight by a factor of 100. The results of this fit are shown in Figure 4.14. Visually, the fitted curves are hardly distinguishable from the previous fit. In order to tease out what the "correct" fit is, more data are needed.

In summary, we have taken a Markov jump process on a state space with 4^{34} states and approximated it by a Markov jump process on only two states. This drastic reduction has allowed us to fit experimental data very quickly compared to running full Gillespie simulations for every feasible set of parameters at each data point. This model is able to fit the available data very well. More experiments are needed to further verify or invalidate it.
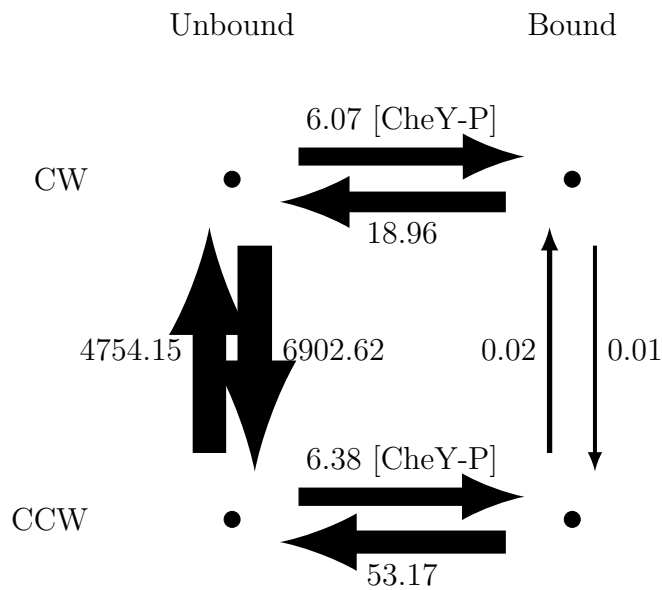
(a) Diagram representing parameter fit for the three aforementioned data sets without weighting them. Here, $\omega = 78.52$.
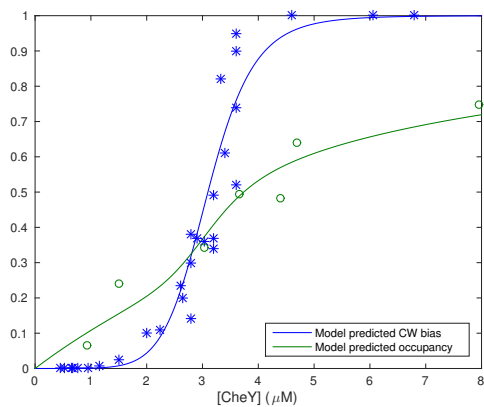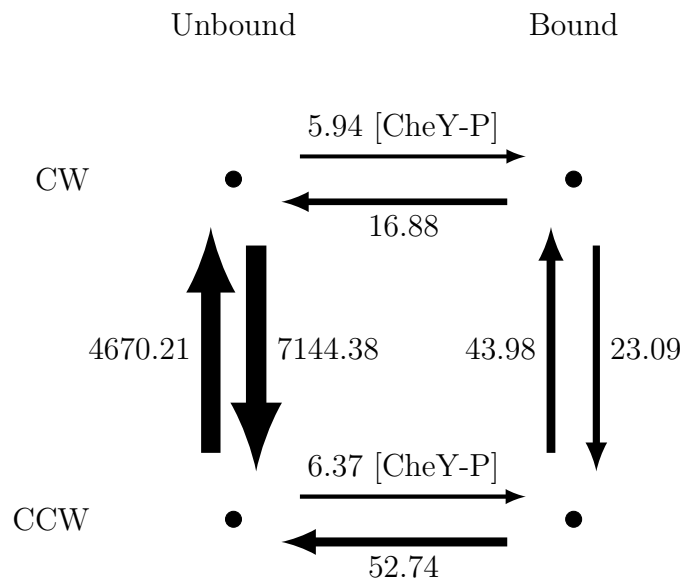

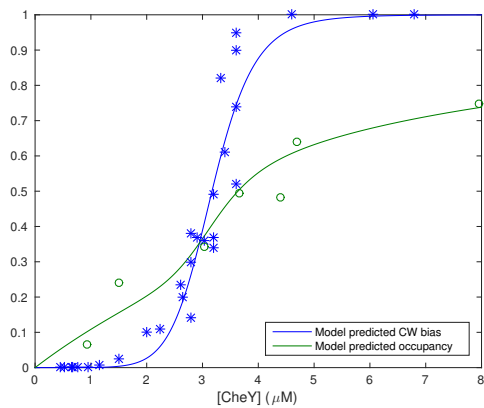(b) Model fit for CW bias data and CheY-P occupancy data.
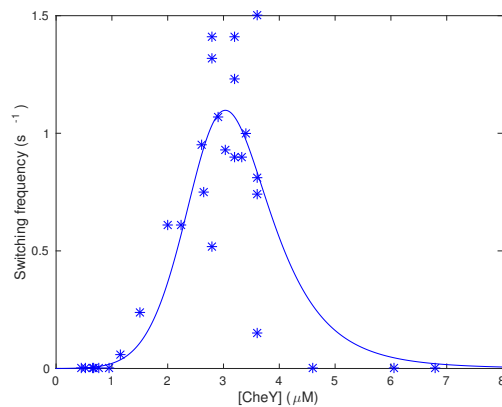
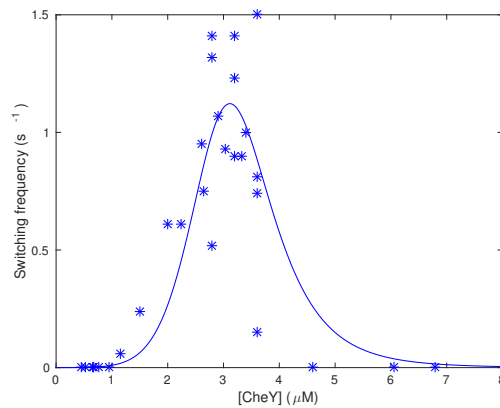(c) Model fit for switching frequency data.

Figure 4.13. Model results for parameter fit to unweighted data.

(a) Diagram representing parameter fit for weighted data. Here, $\omega = 76.61$.

(b) Model fit for CW bias data and CheY-P occupancy data.

(c) Model fit for switching frequency data.

Figure 4.14. Model results for parameter fit to weighted data.

4.3 References

[1] F. Bai, R. W. Branch, D. V. Nicolau Jr., T. Pilizota, B. C. Steel, P. K. Maini, and R. M. Berry, *Conformational spread as a mechanism for cooperativity in the bacterial flagellar switch*, Science, 327 (2010), pp. 685–689.

[2] H. C. Berg, *The rotary motor of bacterial flagella*, Annu. Rev. Biochem., 72 (2003), pp. 19–54.

[3] P. Cluzel, M. Surette, and S. Leibler, *An ultrasensitive bacterial motor revealed by monitoring signaling proteins in single cells*, Science, 287 (2000), pp. 1652–1655.

[4] N. J. Delalez, G. H. Wadhams, G. Rosser, Q. Xue, M. T. Brown, I. M. Dobbie, R. M. Berry, M. C. Leake, and J. P. Armitage, *Signal-dependent turnover of the bacterial flagellar switch protein FliM*, PNAS, 107 (2010), pp. 11347–11351.

[5] T. A. J. Duke, N. Le Novère, and D. Bray, *Conformational spread in a ring of proteins: A stochastic approach to allostery*, J. Mol. Biol., 308 (2001), pp. 541–553.

[6] P. P. Lele, R. W. Branch, V. S. J. Nathan, and H. C. Berg, *Mechanism for adaptive remodeling of the bacterial flagellar switch*, PNAS, 109 (2012), pp. 20018–20022.

[7] Q. Ma, D. V. Nicolau Jr., P. K. Maini, R. M. Berry, and F. Bai, *Conformational spread in the flagellar motor switch: A model study*, PLoS Comput. Biol., 8 (2012).

[8] T. Minamino, K. Imada, M. Kinoshita, S. Nakamura, Y. V. Morimoto, and K. Namba, *Structural insight into the rotational switching mechanism of the bacterial flagellar motor*, PLoS Biol., 9 (2011), p. e1000616.

[9] K. Paul, D. Brunstetter, S. Titen, and D. F. Blair, *A molecular mechanism of direction switching in the flagellar motor of Escherichia coli*, PNAS, 108 (2011), pp. 17171–17176.

[10] K. Paul, G. Gonzalez-Bonet, A. M. Bilwes, B. R. Crane, and D. Blair, *Architecture of the flagellar rotor*, EMBO J., 30 (2011), pp. 2962–2971.

[11] Y. Sagi, S. Khan, and M. Eisenbach, *Binding of the chemotaxis regulator CheY to the isolated, intact switch complex of the bacterial flagellar motor: Lack of cooperativity*, J. Biol. Chem., 278 (2003), pp. 25867–25871.

[12] M. K. Sarkar, K. Paul, and D. Blair, *Chemotaxis signaling protein CheY binds to the rotor protein FliN to control the direction of flagellar rotation in Escherichia coli*, PNAS, 107 (2010), pp. 9370–9375.

[13] V. Sourjik and H. C. Berg, *Binding of the Escherichia coli response regulator CheY to its target measure in vivo by fluorescence resonance energy transfer*, PNAS, 99 (2002), pp. 12669–12674.

[14] Y. Sowa and R. M. Berry, *Bacterial flagellar motor*, Q. Rev. Biophys., 41 (2008), pp. 103–132.

[15] Y. Sowa, A. D. Rowe, M. C. Leake, T. Yakushi, M. Homma, A. Ishijima, and R. M. Berry, *Direct observation of steps in rotation of the bacterial flagellar motor*, Nature, 437 (2005), pp. 196–919.

[16] J. Yuan, R. W. Branch, B. G. Hosu, and H. C. Berg, *Adaptation at the output of the chemotaxis signalling pathway*, Nature, 484 (2012), pp. 233–236.

CHAPTER 5

CONCLUDING REMARKS

The chemical reactions and stochastic processes focused on in this work are only a few of the myriad possible processes that demonstrate contradictory behavior when modeled deterministically or with a mean field approximation. The chemical reaction network theory developed in recent years [1, 3, 2] is useful for gaining an initial understanding of the equilibrium structure of the reaction under consideration. However, we argue that, at the very least, the continuous time, discrete state model of the same process must be considered before monostability can be accepted as the only possible type of behavior the reaction can exhibit.

Even in cases where a state space reduction is not immediately evident, stochastic simulations can yield insight into a possible discrepancy between models. Indeed, in the case of the enzymatic reactions examined in Chapter 2, Gillespie simulations of the reaction produced anomalous distributions which provided the impetus to investigate further. We see that in the case of these enzyme reactions, the deterministic and mean field models predict an equilibrium that is near the mean of the stationary distribution, but that the stationary distribution can be bimodal. The mean of a bimodal distribution is often far from states that occur with any appreciable probability. Thus, the deterministic prediction may not be useful for understanding observed concentrations in laboratory experiments.

In the case of the autocatalytic reactions in Chapter 3, Gillespie simulations do, in fact, appear to coincide with the predicted steady states from the deterministic model, because the stationary distributions of these chemical master equations require very long times to reach, as long as the initial condition of the simulation is not the stationary distribution itself.

Finally, in considering the rotation direction switching of the bacterial flagellar motor in Chapter 4, we see that a mean field approach to modeling the number of CW versus CCW subunits does not account for important neighbor-neighbor interactions. In effect, the proportion of CW subunits cannot be treated like a homogeneous concentration of the total. We also see that the number of subunits plays an important role in determining the sensitivity of the switch.

5.1   Future Directions

The reduction of the state space of the motor is the tool that allows us to quickly and efficiently sample a large portion of parameter space to find the best fit. With the data currently available, this best fit is not unique. More experiments will need to be performed in order to narrow the range of acceptable rate constants, though, at the current time, we do not know what experiments may be useful in this endeavor.

Another observation from our work is that there is much yet to be done to generalize the state space reduction approach to analyzing the chemical master equation. The solution of the chemical master equation may be the most accurate description of chemical reactions. We believe that the reduction of large or infinite state spaces will prove to be a key step toward increasing the usefulness of the chemical master equation.

Ultimately, the goal in developing these tools, in this particular context, is to be able to use them to increase our understanding of reaction network behavior. The species-reaction graph is a powerful tool for determining properties of the resultant deterministic system, but, as of yet, it can say nothing about the stochastic process a chemical reaction really is.

5.2   References

[1] G. Craciun and M. Feinberg, *Multiple equilibria in the complex chemical reaction networks: I. The injectivity property*, SIAM J. Appl. Math., 65 (2005), pp. 1526–1546.

[2] ——, *Multiple equilibria in the complex chemical reaction networks: Extensions to entrapped species models*, IEE Proc. Systems Biol., 153 (2006), pp. 179–186.

[3] ——, *Multiple equilibria in the complex chemical reaction networks: II. The species-reaction graph*, SIAM J. Appl. Math., 66 (2006), pp. 1321–1338.